

AD-A039 992

RCA LABS PRINCETON N J
INJECTION LASER FOR HIGH DATA RATE COMMUNICATIONS.(U)
APR 77 J P WITTKE, I LADANY, H KRESSEL

F/G 20/5

N00014-76-C-0709

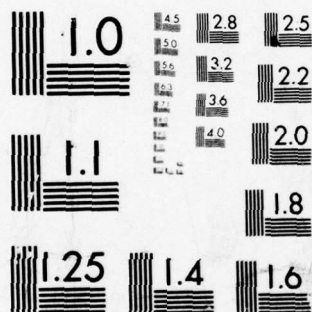
UNCLASSIFIED

PRRL-77-CR-13

NL

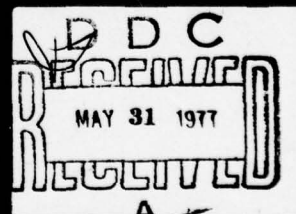
1 OF 1
AD
A039 992





MICROCOPY RESOLUTION TEST CHART
NATIONAL BUREAU OF STANDARDS-1963-A

ADA 039992



DISTRIBUTION STATEMENT A
Approved for public release
Distribution Unlimited

UNCLASSIFIED

SECURITY CLASSIFICATION OF THIS PAGE (When Data Entered)

REPORT DOCUMENTATION PAGE		READ INSTRUCTIONS BEFORE COMPLETING FORM
1. REPORT NUMBER	2. GOVT ACCESSION NO.	3. RECIPIENT'S CATALOG NUMBER
TITLE (and Subtitle)		5. TYPE OF REPORT & PERIOD COVERED
INJECTION LASER FOR HIGH DATA RATE COMMUNICATIONS.		Final Report (3-1-76 to 2-28-77) ✓
7. AUTHOR(s)		6. PERFORMING ORG. REPORT NUMBER
Wittke, ✓ Ladany, ✓ Kressel		PRRL-77-CR-13 ✓
9. PERFORMING ORGANIZATION NAME AND ADDRESS		8. CONTRACT OR GRANT NUMBER(s)
RCA Laboratories Princeton, New Jersey 08540		N00014-76-C-0709 ✓
11. CONTROLLING OFFICE NAME AND ADDRESS		10. PROGRAM ELEMENT, PROJECT, TASK AREA & WORK UNIT NUMBERS
Office of Naval Research Department of the Navy Arlington, Virginia 22217		
14. MONITORING AGENCY NAME & ADDRESS (if different from Controlling Office)		12. REPORT DATE
Final rept. 1 Mar 76-28 Feb 77		Apr 77
		13. NUMBER OF PAGES
		49
		15. SECURITY CLASS. (of this report)
		Unclassified
		15a. DECLASSIFICATION/DOWNGRADING SCHEDULE
		N/A
16. DISTRIBUTION STATEMENT (of this Report)		
Distribution in whole or in part is permitted for any purpose of the United States Government.		
17. DISTRIBUTION STATEMENT (of the abstract entered in Block 20, if different from Report)		
DISTRIBUTION STATEMENT A Approved for public release; Distribution Unlimited		
18. SUPPLEMENTARY NOTES		
19. KEY WORDS (Continue on reverse side if necessary and identify by block number)		
Injection lasers Laser-fiber coupling Laser modes Fiber pigtail Single-mode fiber		
20. ABSTRACT (Continue on reverse side if necessary and identify by block number)		
<p>Injection lasers of AlGaAs ($\lambda \approx 800$ nm) have been permanently bonded to single-mode fibers, with power levels up to 600 μW being coupled into the fibers. Values over 150 μW were consistently obtained under cw operation at room temperature. Very close mechanical alignment tolerances are required to achieve good coupling, with positioning to $\pm 1 \mu$m being required. This necessitates the use of bonding materials for attaching the fiber to the laser mount</p>		

DD FORM 1473
1 JAN 73

micrometer

UNCLASSIFIED

SECURITY CLASSIFICATION OF THIS PAGE (When Data Entered)

CDE 299 004

microwatts

next page

DDC
RECEIVED
MAY 31 1977
RECEIVED
A

UNCLASSIFIED

SECURITY CLASSIFICATION OF THIS PAGE (When Data Entered)

20.

cont

→ that have a high dimensional stability over long time periods, and lasers whose modal patterns do not change with time or operating conditions. An epoxy provided the best bonding material that we found, although there are indications that suitable low-melting solders can also be used. Laser mode changes with drive current level can alter the observed coupling efficiency significantly. ↑

UNCLASSIFIED

SECURITY CLASSIFICATION OF THIS PAGE (When Data Entered)

PREFACE

This Final Report describes research performed during the period 1 March 1976 through 28 February 1977, under Contract N00014-76-C-0709, at RCA Laboratories in the Materials Research Laboratory, Dr. James J. Tietjen, Director, and the Systems Research Laboratory, Mr. Nathan L. Gordon, Director. The Project Supervisor was Dr. Henry Kressel and the Project Scientist was Dr. James P. Wittke, with Mr. Ivan Ladany participating in the research effort. The Navy Project Monitor was Dr. Theodore Pavlopoulos.

ACCESSION	
STC	With Section <input checked="" type="checkbox"/>
DS	With Section <input type="checkbox"/>
UNCLASSIFIED	<input type="checkbox"/>
<i>Wittke on file</i>	
BY	
DISTRIBUTION AVAILABILITY CODES	
UNCL	AVAIL. CODE SPECIAL
A	

TABLE OF CONTENTS

Section	Page
I. INTRODUCTION	1
II. LASER DIODE STRUCTURES	3
III. LASER RELIABILITY	7
IV. LASER MODES	11
A. Geometrical Considerations	11
B. Detailed Analysis of a Laser	13
V. RADIATION COUPLING	25
VI. MECHANICAL CONSIDERATIONS	31
VII. FIBER-LASER ASSEMBLIES;RESULTS	37
VIII. CONCLUSIONS	40
REFERENCES	42

LIST OF ILLUSTRATIONS

Figure		Page
1.	Schematic cross section of double-heterojunction laser used in the present work	3
2.	The ratio of the stripe threshold current density to the broad-area threshold current density as a function of normalized stripe contact width	5
3.	Experimental measurements of the ratio of stripe-threshold to broad-area-threshold current densities for various stripe widths for three groups of diodes. Also shown are calculated curves from the theory given in the text	6
4.	Reflectivity of a dielectric film of refractive index n_2 as a function of its optical thickness, n_2h , when it is deposited on a GaAs substrate of index $n_3 = 3.6$. Several values of film index n_2 are shown	8
5.	Measured and calculated reflectivities for aluminum oxide films on GaAs as a function of film thickness, assuming the index of the film is $n = 1.72$	9
6.	Laser lifetime test results. The optical output power from several representative groups of lasers is shown as a function of time, for coated and (one) uncoated lasers. The lasers were driven at constant current, with a constant heat sink temperature	9
7.	Near-field radiation patterns (at the laser facet) of two lasers that exhibit different kinds of "kinks" in their power output-drive current curves. (a) A laser with a kink related to mode changes; (b) A laser showing filamentary lasing due to poor metallurgical control during layer growth. Also shown are the power curves for these lasers	14
8.	Power output curve for a laser, showing a mode change-related kink. Also shown are the noise peaks (at 60 MHz) associated with the onset of lasing at the 335-mA threshold and with the start of oscillations in a second lateral mode at the kink at 370 mA . . .	16
9.	Far-field radiation patterns of the laser of Fig. 8 at two power levels. At the 9-mW level, (below the kink), only one lateral mode is oscillating; at 20 mW, (above the kink), two lateral modes are seen	17
10.	The observed far-field mode pattern of the second lateral mode, after that of the fundamental mode has been subtracted out as explained in the text. The dashed line shows the pattern expected for the first higher-order Hermite-Gaussian mode	18
11.	Relative power output curves for the laser of Fig. 8 taken at three angles (in the far-field) with respect to the laser beam axis. The dashed lines are an extrapolation of the off-axis single-mode parts of the curves into the two-mode regions. The power saturation in the fundamental lateral mode is evident	19

LIST OF ILLUSTRATIONS (Continued)

Figure	Page
12. Optical spectra of the laser of Fig. 8 at two power levels. (a) Output power 6 mW, (below kink). Only longitudinal modes associated with the fundamental lateral mode (A) are seen. (b) Output power 16 mW, (above kink). Longitudinal modes associated with both the fundamental lateral mode (A) and first higher order lateral mode (B) are seen	21
13. Wavelength of the longitudinal mode of maximum intensity in the fundamental lateral mode as a function of laser drive current . . .	23
14. Measured beam profile of radiation transmitted through a section of mode-stripped single-mode fiber, taken at 806 nm using a cw injection laser. The data points represent the measured profile scanned across the center of the far-field radiation pattern; the solid curve shows a Gaussian profile	26
15. Change of coupling from laser into single-mode fiber as the fiber end is translated perpendicular to the beam axis. Displacements in, (), and perpendicular to, (⊥), the junction plane are shown. (a) Coupling variations for a laser with a 5- μ m-wide stripe electrical contact; (b) Coupling variations for a laser with a 13- μ m-wide stripe contact	29
16. Coupling efficiency as a function of laser power for lasers with different contact stripe widths	30
17. Cross section of the laser-fiber mounting package	32
18. Far-field laser radiation patterns at two different temperatures and peak output powers, taken under pulsed conditions. Pulse length = 0.5 μ s	35
19. Far-field laser radiation patterns taken at a constant ($T = 23^{\circ}\text{C}$) heat-sink temperature. (Arbitrary normalizations.) Patterns taken under both cw and pulsed conditions are shown. At lower pulse current conditions than shown, the peak remained at -4° , but the pattern broadened significantly. At higher pulse currents than shown, the peak shifted to even more negative angles than for 300 mA.	36
20. Output power through a coupled single-mode fiber for one laser-fiber unit. A current of 180 mA corresponds to a total laser output power of 10 mW	38
21. Output power through a coupled single-mode fiber for a second laser-fiber unit. A current of 195 mA corresponds to a total laser output of 10 mW	39

SECTION I

INTRODUCTION

With multimode fibers, as the data rate in an optical fiber communications system is increased into the gigabit/second range, modal dispersion, mode coupling, and differential loss problems limit the distance that a signal can usefully propagate before regeneration is required. Fiber dispersion problems can be greatly alleviated at these high data rates by using a single-mode fiber. However, the choice of such a propagation medium leads to a host of related problems. One of the most severe is that of developing means of reliably coupling the light from an injection laser source into the small diameter ($<10\text{ }\mu\text{m}$) single propagating fiber mode. Lasers whose characteristics are optimized for this characteristic must then be considered from the point of reliability and power output.

Because of the extremely small core diameter required to ensure that a fiber is able to propagate only one mode, very small deviations from optimum alignment, especially transverse displacements of the fiber relative to the laser in a direction normal to the junction plane, lead to rapid decreases in coupled power. This means that the package used to maintain the laser-fiber positions must be dimensionally stable. Thus, the laser package must be designed to minimize thermal distortions and stable materials must be used in bonding the fibers into position near the lasers.

The objective of the program described in this report was to develop devices and methods of permanently coupling cw laser diode sources to single-mode fibers. The problems were:

- (1) Reliability aspects of the laser diode itself, and the relationship between the power emitted and the source size.
- (2) Factors affecting the modes of the laser as they determine coupling efficiency into single-mode fibers.
- (3) Mechanical aspects of the assembly, which consists of the laser and the fiber permanently attached in a practical package.

The program has been successfully completed, and permanent single-mode-fiber "pigtail" structures have been developed. However, a number of difficulties remain with regard to such assemblies which could lead to changes (over long periods of time) in the fraction of the power from the laser coupled into the fiber.

The devices used for this work were AlGaAs laser diode structures of the type previously developed at RCA Laboratories [1], with modifications introduced to improve their coupling to single-mode fibers. These lasers emit at $\sim 0.8 \mu\text{m}$, a wavelength desirable for low attenuation in present fibers.

-
1. I. Ladany and H. Kressel, "Influence of Device Fabrication Parameters on Gradual Degradation of (AlGa)As CW Laser Diodes," Appl. Phys. Lett. 25, 708 (1974).

SECTION II

LASER DIODE STRUCTURES

Since the fiber core has a diameter of about $8\text{ }\mu\text{m}$, the power emitted by the laser diode in a source width of that size evidently determines the maximum cw power level available for coupling. In this regard, there are two options: (1) produce a laser diode with a source width equal to or smaller than the fiber diameter; or (2) produce wider lasers, but only couple the power available from the $8\text{-}\mu\text{m}$ -wide region at the center of the device.

The approach taken in this program was to base the work on the cw laser diode structure which in our previous work demonstrated outstanding reliability (Section III). This device, shown in Fig. 1, consists of a double-heterojunction of $\text{Al}_{0.3}\text{Ga}_{0.7}\text{As}/\text{Al}_{0.1}\text{Ga}_{0.9}\text{As}$, with the stripe contact defined by oxide isolation. Many different stripe contact technologies have been reported in the literature; our selection of this particular one is based on the fact that it minimizes the possibility of introducing damaging lattice defects in the course of fabrication. However, its degree of lateral current and radiation confinement is not high; it produces an active region width in the plane of the junction that can substantially exceed the stripe width.

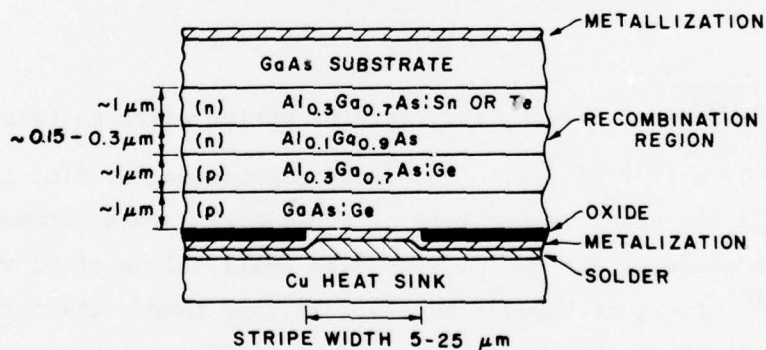


Figure 1. Schematic cross section of double-heterojunction laser used in the present work.

One of the reasons for the increase in threshold current density of a stripe laser is that the current spreading beyond the edge of the contact reduces the injection level into the active region under the contact. Another is the loss of carriers from under the stripe due to lateral diffusion (out-diffusion). In addition, the radiation spreads into lossy regions adjoining the stripe edge, producing an effective absorption coefficient for the propagating modes which exceeds the value in a device with homogeneous population inversion and strong lateral dielectric walls.

The effect of the current spread on the carrier outdiffusion, and thereby on threshold current, has been calculated [2], and the results are presented as a set of curves in Fig. 2, giving the ratio of the threshold current density of the stripe lasers (J_s) compared to the threshold current density J_0 of a similar device where the (wide) stripe area would truly represent the total cavity area. Hence, the ratio shown in Fig. 2 represents the penalty resulting from the partial carrier loss in the stripe contact device. The key parameter controlling the current spread is the sheet resistance of the material between the metal contact and the edge of the recombination region. The ratio J_s/J_0 follows the form

$$\frac{J_s}{J_0} = \frac{1 + \frac{Q}{w'}}{1 + \exp(-w') \cdot F(Q)} \quad (1)$$

where $Q \equiv \frac{1}{L} \sqrt{\frac{2mkT}{R_s J_0 q}}$; $w' \equiv w/2L$, the ratio of stripe width to twice the diffusion length, and $F(Q) \approx [1 + \frac{2}{Q}]^{-1} - 1$. (The exact expression for $F(Q)$ is given in Ref. 2.) R_s is the sheet resistivity of the p-type layers between the junction and the stripe contact, and $m \approx 2$. For very small values of w , we have $J_s/J_0 \approx \frac{2(Q+2)L}{w}$, i.e., it behaves as $1/w$. In this range, the threshold current density increase is exactly compensated by the width reduction, there being no change in threshold current as the diode is made narrower.

2. I. Ladany, "The Influence of Stripe Width on the Threshold Current of DH Lasers," J. Appl. Phys. (to be published).

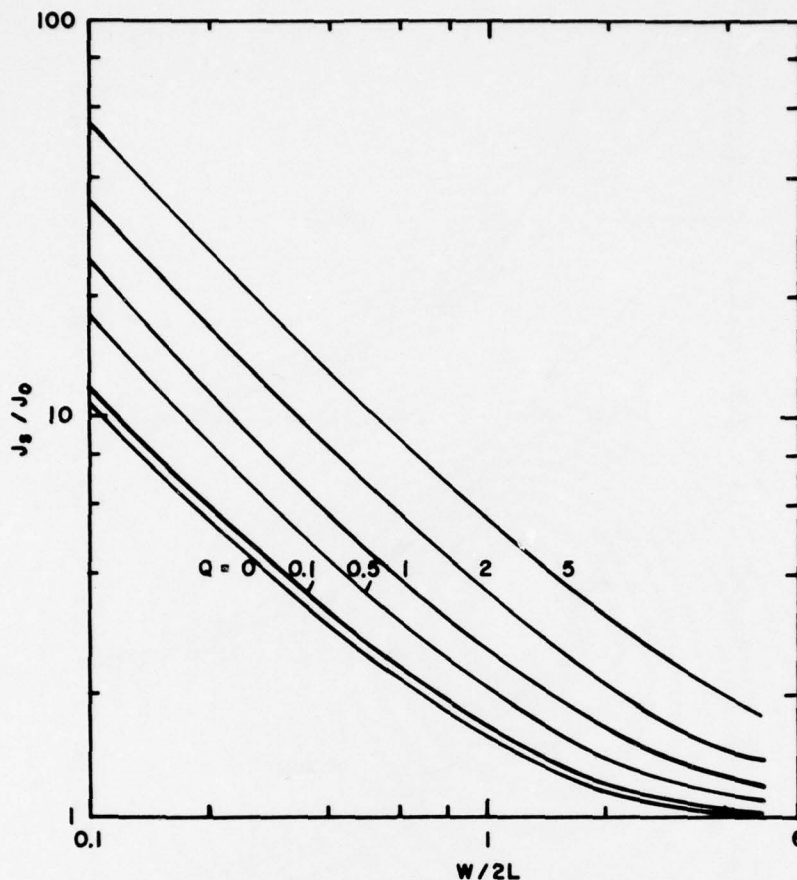


Figure 2. The ratio of the stripe threshold current density to the broad-area threshold current density as a function of normalized stripe contact width.

Experimental measurements superimposed on the calculated values are shown in Fig. 3 for three sets of data. Below $w/2L \approx 0.6$ the threshold ratio rises far above that predicted by the equation. This increase is believed due to optical losses which occur when the wave spreads beyond the pumped region.

The diffusion length is an adjustable parameter in this calculation, but a value of $\approx 7 \mu\text{m}$ yields reasonable agreement between calculation and experiment for our devices.

The conclusion from these calculations and experiments is that the narrowest stripe width before the threshold current increases "excessively" is $w \approx 8 \mu\text{m}$. In the present work, stripe widths of ≈ 5 to $\approx 25 \mu\text{m}$ were studied from the point of view of fiber coupling and mode control. However, the actual extent of the emitting region was wider than the stripe width for the narrow stripe values.

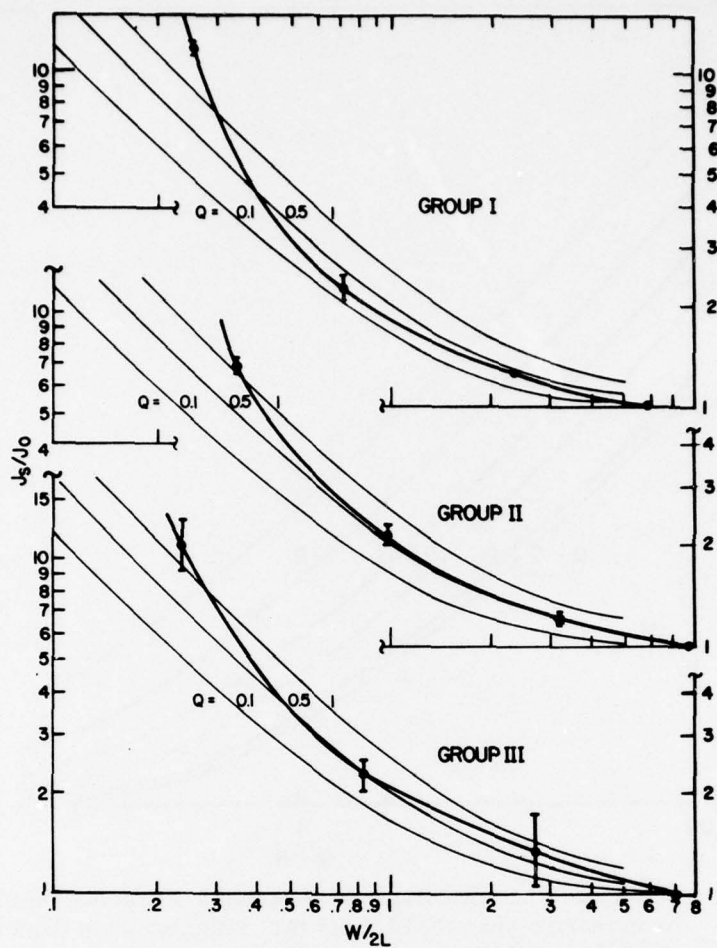


Figure 3. Experimental measurements of the ratio of stripe-threshold to broad-area-threshold current densities for various stripe widths for three groups of diodes. Also shown are calculated curves from the theory given in the text.

SECTION III

LASER RELIABILITY

Laser reliability is known to be affected by three basic factors. The first is internal degradation, where lattice defects are formed as a result of electron-hole recombination. These nonradiative centers are either isolated or clustered and reduce the internal quantum efficiency. Our previous work at RCA Laboratories has shown that this process of degradation is negligible in the 10,000-h time frame for properly fabricated lasers. The second degradation mode is rapid facet damage (catastrophic degradation) resulting from a high optical flux density. We have established that in lasers with a 15- μm stripe width, catastrophic damage is induced at the 30 to 40 mW power level. The third degradation process is facet erosion. This can occur over many thousands of hours of operation [3,4]. This process is related to the optical field intensity of the facet and the ambient conditions. Moisture, for example, accelerates facet erosion.

Facet erosion is controlled by the passivation of the facet with a suitable half-wave-thick dielectric material. We have found that Al_2O_3 is very useful [3,4], and we have obtained excellent reliability with such coatings operating at a typical power emission level of 1 mW/ μm of effective stripe width (giving, typically, 10 to 15 mW). Table 1 shows three materials investigated for facet coatings, with the methods of deposition and the problems encountered.

Figure 4 shows a set of curves illustrating the way the reflectivity of the interface changes with film thickness and the refractive index of the coating. Figure 5 shows experimental data for Al_2O_3 films superimposed on the calculated curve using $n = 1.72$ for the index of Al_2O_3 , and 3.6 for the index of GaAs.

3. H. Kressel and I. Ladany, "Reliability Aspects and Facet Damage in High-Power Emission from (AlGa)As CW Laser Diodes at Room Temperature," RCA Rev. 36, 230 (1975).
4. I. Ladany, M. Ettenberg, H. F. Lockwood, and H. Kressel, " Al_2O_3 Half-Wave Films for Long-Life CW Lasers," Appl. Phys. Lett. 30, 87 (1977).

TABLE 1. MATERIALS FOR FACET COATINGS

Coating	Deposition	RESULTS		
		Mechanical	Optical	Degradation Resistance
SiO_x	thermal evaporation	occasional peeling	high index	poor, not stable against H_2O
Borosilicate glass	sputtering	tendency to crack when processing material	very desirable because of low index	very good
Al_2O_3	electron beam evaporation	very good adhesion	sensitive to optical path length	very good

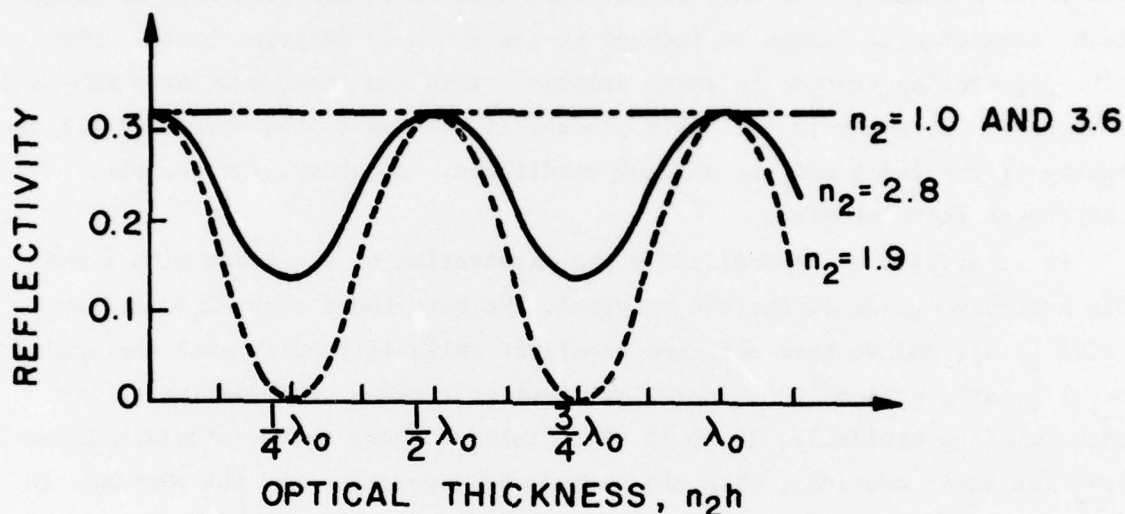


Figure 4. Reflectivity of a dielectric film of refractive index n_2 as a function of its optical thickness, n_2h , when it is deposited on a GaAs substrate of index $n_3 = 3.6$. Several values of film index n_2 are shown.

Figure 6 shows the results of cw laser life tests of groups of lasers with Al_2O_3 facet coatings. The stability is seen to be excellent, and the fact that the diode tests are at constant current indicates that the actual device changes are minimal. Also shown in Fig. 6 is the life test result of a laser selected from one of the groups tested, but without facet passivation. This laser, as was the case with the others, was operated in a laboratory ambient, i.e., without any attempt made to control the ambient conditions. The reduction in the output from the laser is due to facet erosion which decreases the reflectivity

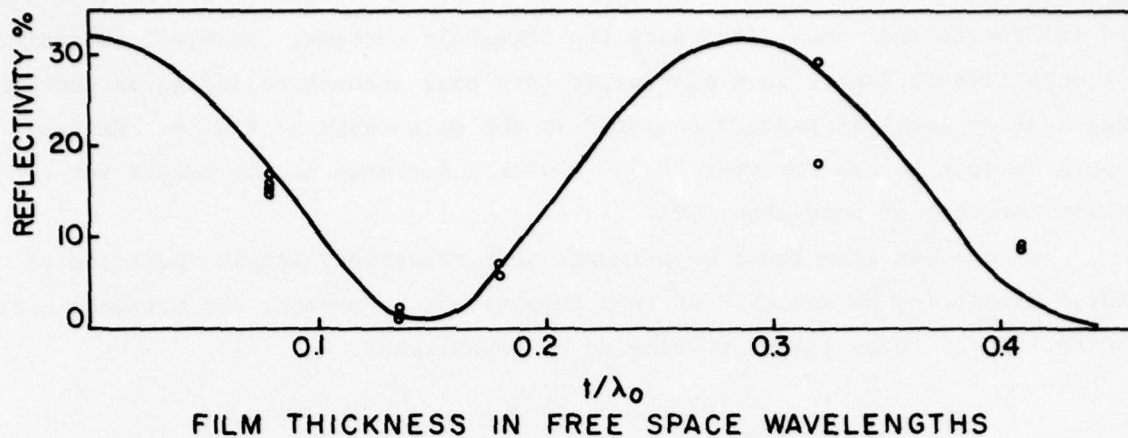


Figure 5. Measured and calculated reflectivities for aluminum oxide films on GaAs as a function of film thickness, assuming the index of the film is $n = 1.72$.

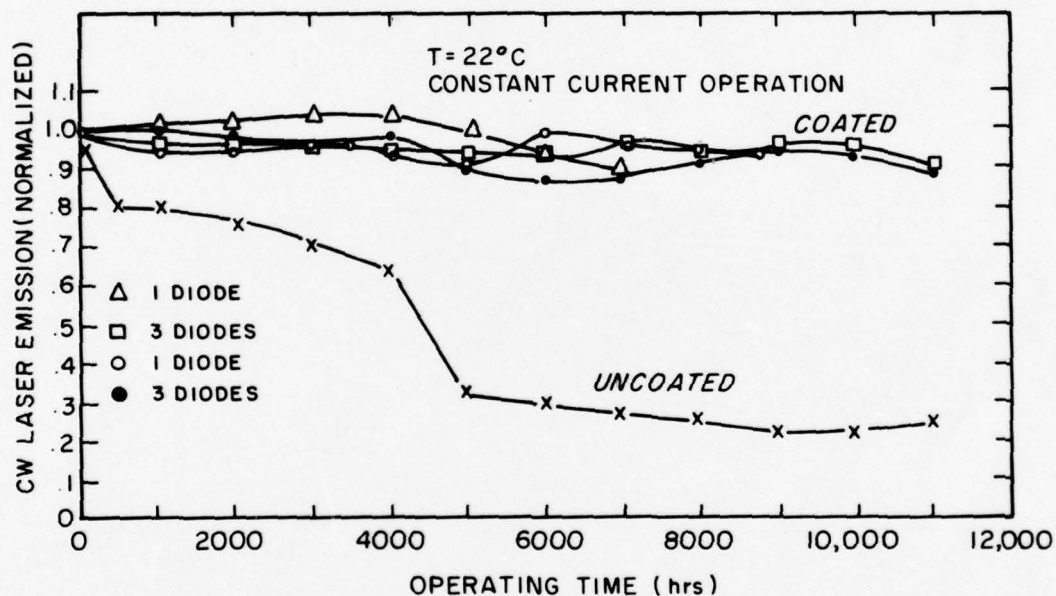


Figure 6. Laser lifetime test results. The optical output power from several representative groups of lasers is shown as a function of time, for coated and (one) uncoated lasers. The lasers were driven at constant current, with a constant heat sink temperature.

of the facets and, thus, increases the threshold current. However, operation of unpassivated lasers in a controlled (dry box) atmosphere indicates that the degradation level is reduced compared to the data shown in Fig. 6. We have operated such lasers for over 24,000 h with a decrease in the output (at constant current) of only about 40%.

We conclude from these experiments that relatively stable operation of laser diodes may be achieved at room temperature. However, the ultimate operating life of these lasers remains to be established.

SECTION IV

LASER MODES

A. GEOMETRICAL CONSIDERATIONS

The laser radiation pattern controls the coupling efficiency into single-mode fibers. The beam in the direction perpendicular to the junction plane is controlled by the transverse cavity modes, while the beam in the junction plane is controlled by the lateral modes. All of our devices operate in the fundamental transverse mode, with the beam width being determined by the width of the heterojunction spacing, d , and the index steps at the heterojunctions. These are related to the difference in the Al concentrations ($x-y$) at the $\text{Al}_{1-x}\text{Ga}_x\text{As}/\text{Al}_{1-y}\text{Ga}_y\text{As}$ boundaries by the experimental relationship

$$\Delta n = 0.62 (x-y) \quad (2)$$

The need to minimize the threshold current density places a lower limit on Δn because excessively low barriers result in an undesirable temperature sensitivity of the threshold current density as well as too high an initial threshold density. For the present devices, a nominal width $d = 0.2 \mu\text{m}$ was used, with ($x-y$) in the range 0.2 to 0.25. The predicted beam width is about 40° , which is indeed typical of measured values for our lasers.

The control of the lateral modes of semiconductor lasers is complicated by the mode proliferation commonly observed with increasing current above threshold. In principle, it is possible to restrict operation to the desirable fundamental lateral mode, but only if diode width is sufficiently narrow. Assuming a laser configuration with two dielectric steps confining the current and the radiation in the junction plane, the required index step, Δn , is related to the junction width, w , by

$$\frac{\Delta n}{n} \lesssim \frac{1}{8} \left(\frac{\lambda}{nw} \right)^2 \quad (3)$$

For a device with pure GaAs or with a small Al concentration in the recombination region, $n \approx 3.6$ and the fundamental mode condition is

$$\frac{\Delta n}{n} \lesssim \frac{7.8 \times 10^{-3}}{w^2} \quad (4)$$

where w is in micrometers.

For example, if the sides of the diodes are etched, the air-GaAs interface would have an index step $\Delta n/n = 0.72$, and we would have to restrict the diode width to $w \approx 0.1 \mu\text{m}$ to maintain fundamental mode operation. Since this dimension is obviously too small, the use of etched mesa diodes to confine the oscillation to the fundamental lateral mode is not a viable approach.

The use of the buried heterojunction construction [5] is an alternative method of achieving narrow stripe lasers with steep dielectric walls. Assuming the buried heterojunction index step to be $\Delta n \approx 0.0062$, if fundamental mode operation is desired, the effective diode width has to be restricted to $\approx 1 \mu\text{m}$, which limits the cw power emitted. Since a safe power level is approximately 1 mW of cw power per micrometer of diode width, a 1- μm -wide diode would only emit about 1 mW, a value considered to be too low for the present application. As discussed below, the fiber would be located in the far-field region of such a laser source, and the lateral beam width of such a structure would be very wide. This would result in a very low coupling efficiency, -18 dB, or less.

In planar stripe lasers, such as the oxide-isolated ones used in our work, the index profile controlling the mode guiding in the junction plane is largely self-induced, being dependent on the gain and the current distribution. Changes in the current distribution with drive can, therefore, perturb the index distribution and hence change the lateral modes that are observed. These mode changes are reflected in two characteristics:

- (1) Broadening of, and/or structure in, the far-field radiation pattern in the junction plane.
- (2) Slope changes in the power vs drive current curve. However, the "kinks" observed in these curves can have different origins.

5. Y. Tsukada, "GaAs-Ga_{1-x}Al_xAs Buried-Heterostructure Injection Lasers," J. Appl. Phys. 45, 4899 (1974).

Figure 7 shows examples of two types of kinks in a power curve in cw operation. Laser A has a relatively uniform near-field radiation pattern and exhibits a kink which was determined to be related to a change in the lateral modes. Laser B, on the other hand, has a filamentary near-field pattern characteristic of poor diode metallurgy, and the kink is clearly of a different origin. We shall be concerned here with kinks in the curves relating to mode changes, since the other types of kinks are basically metallurgical in origin and can, therefore, be controlled by the use of sufficiently uniform material. In the following section we describe the characteristics of one laser which we analyzed in detail with regard to the relation of the kink to the modes as well as the radiation pattern in the plane of the junction.

B. DETAILED ANALYSIS OF A LASER

To illustrate the complexity of the mode situation in injection lasers, in this section we report on the characteristics of a laser which was studied in detail. This device shows many regularities of performance, but all the measurements reported herein, taken together, cannot be consistently interpreted in terms of available theories. We present data on output power as a function of drive current, the concomitant low frequency noise characteristics, near- and far-field beam patterns and spectra.

The laser was grown by our standard liquid phase epitaxial techniques. In the recombination region ($d = 0.15 \mu\text{m}$) the composition $\text{Al}_x\text{Ga}_{1-x}\text{As}$ had an aluminum concentration $x \approx 0.1$, giving output wavelengths near $806 \mu\text{m}$. This region was not intentionally doped. It was between two heterojunctions with $x \approx 0.3$ material outside the active region. The laser operated in the fundamental transverse mode, with a far-field beam width perpendicular to the junction plane of 42° . The SiO_2 -isolated contact stripe was $25 \mu\text{m}$ wide; the laser length was $406 \mu\text{m}$. For such wide stripes, the effective width is very close to the stripe width.

The low-frequency noise characteristics were measured by using a set-up similar to that reported by Paoli [6], modified by the replacement of the

6. T. L. Paoli, "Noise Characteristics of Stripe-Geometry Double-Heterostructure Junction Lasers Operating Continuously - I. Intensity Noise at Room Temperature," IEEE J. Quantum Electron. QE-11, 276 (1975).

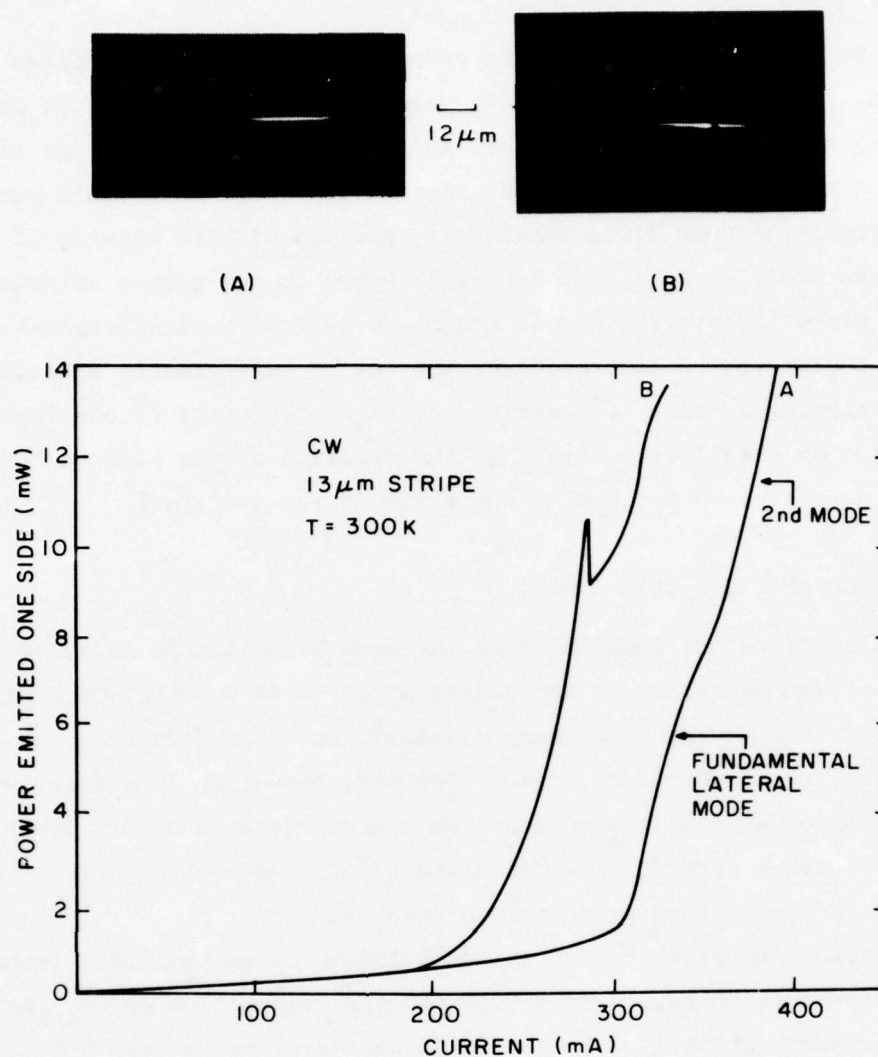


Figure 7. Near-field radiation patterns (at the laser facet) of two lasers that exhibit different kinds of "kinks" in their power output-drive current curves.

(a) A laser with a kink related to mode changes;

(b) A laser showing filamentary lasing due to poor metallurgical control during layer growth.

Also shown are the power curves for these lasers.

spectrum analyzer by a Nems Clarke Model 1302 special-purpose receiver. This was operated at a frequency of 60 MHz, well below the expected laser "spiking resonances" [7,8], with a bandwidth of 300 kHz. Near-field radiation patterns (at the emitting laser facet) were observed through a microscope with a vidicon pick-up and TV monitor display. Optical filters were used to ensure that the system was operating in a linear mode. Far-field patterns were detected with a photomultiplier scanned in the plane of the laser junction, with a 10-mrad acceptance aperture. Optical spectra were measured on a conventional grating spectrometer with a resolution of 0.01 nm.

Figure 8 shows the power curve for (one emitting facet of) the laser. The kink observed at an output of 12 mW is identified with the onset of a second lasing lateral mode. The details of what occurs at this power level will be discussed below. One indication that a new mode-group begins to oscillate here is also shown on Fig. 8, where the relative noise power [6] for the laser is also plotted. It is seen that there are two distinct "noise peaks," with noise-quieting between them. The first peak is associated with the laser threshold, and the second with the kink in the power curve. Such behavior would be expected from the turning-on of two independent van der Pol oscillators.[9]

The possibility that the kink indicated the onset of a second laser oscillation mode was further examined by a scan of the far-field radiation pattern at power levels above and below that of the kink. Such data are shown in Fig. 9. Between the laser threshold and the kink, the far-field pattern is quite accurately Gaussian. This would be expected if the stripe-contact geometry led to a parabolic effective index of refraction variation in the lateral direction (plane of the junction) [10]. The rate at which the index, n , would have to fall off to give the observed angular beam spread, is

7. D. E. McCumber, "Intensity Fluctuations in the Output of CW Laser Oscillators-I," Phys. Rev. 141, 306 (1966).
8. T. L. Paoli and J. E. Ripper, "Observation of Intrinsic Quantum Fluctuations in Semiconductor Lasers," Phys. Rev. 2A, 2551 (1970)
9. J. A. Armstrong and A. W. Smith, "Intensity Fluctuations in GaAs Laser Emission," Phys. Rev. 140, A155 (1965).
10. T. H. Zachos and J. E. Ripper, "Resonant Modes as GaAs Junction Lasers," IEEE. J. Quantum Electron. QE-5, 29 (1969).

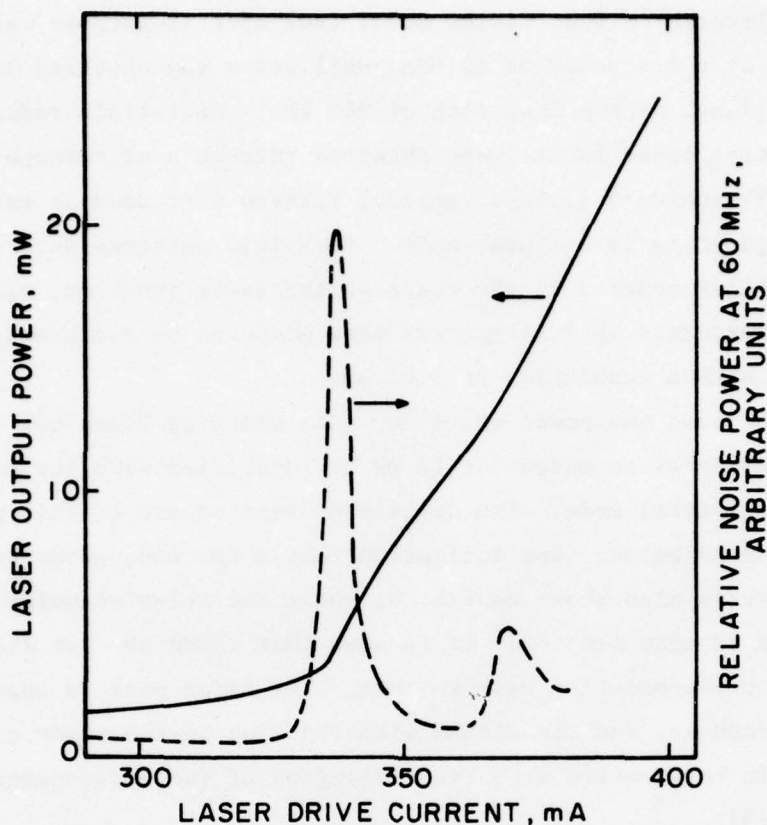


Figure 8. Power output curve for a laser, showing a mode change-related kink. Also shown are the noise peaks (at 60 MHz) associated with the onset of lasing at the 335-mA threshold and with the start of oscillations in a second lateral mode at the kink at 370 mA.

$$n = \bar{n} \left[1 - \left(\frac{y}{y_e} \right)^2 \right]^{1/2} \quad (5)$$

(measured from $y = 0$ at the center of the contact stripe, with $y_e = 1388 \mu\text{m}$.)

At output powers $>12 \text{ mW}$, i.e., above the kink, the beam pattern changes to the double-peaked curve also shown in Fig. 9. Subtracting out (as indicated below) the Gaussian component from this second curve, one obtains the result shown in Fig. 10. This curve, except near the expected central null, is well fit by the first order Hermite-Gaussian (H-G) function with the same angular width parameter, and, hence, is the expected first higher-order mode of a parabolic-index cavity resonator.

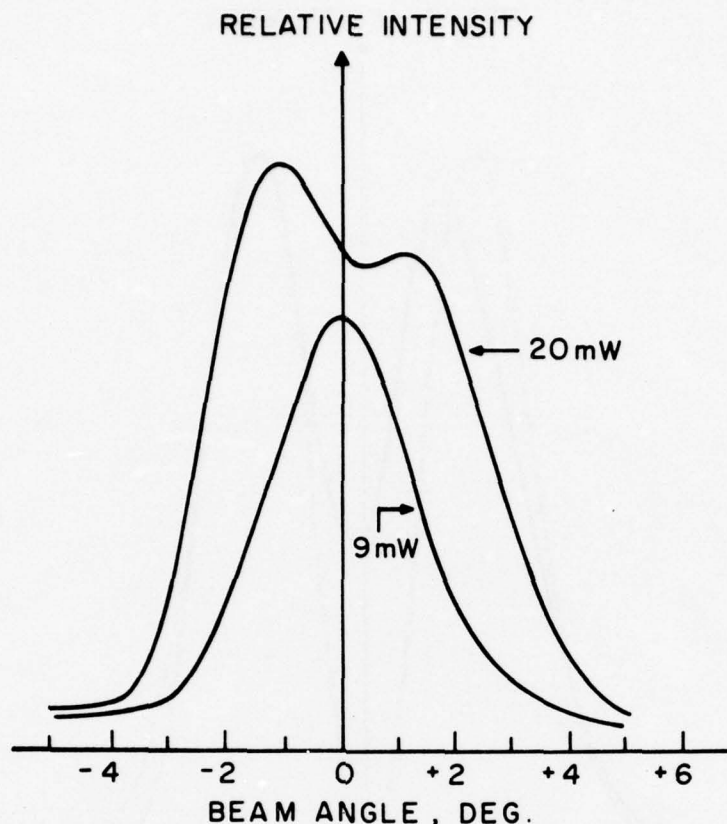


Figure 9. Far-field radiation patterns of the laser of Fig. 8 at two power levels. At the 9-mW level, (below the kink), only one lateral mode is oscillating; at 20 mW, (above the kink), two lateral modes are seen.

Below the kink, the lowest-order modes show evidence of saturation. To explore this, we measured a (relative) power curve at $\theta = 0^\circ$, accepting only light within 10 mrad of the center of the Gaussian peak, and also curves at $\theta = \pm 2^\circ$, where the first-order H-G modes have considerably greater intensity than the fundamental modes. The results are shown in Fig. 11. The power into the fundamental modes is seen to saturate; by comparing this curve to that part of Fig. 8 below the kink, (and subtracting out the extrapolated, incoherent, spontaneous emission), the saturated power level for these fundamental modes can be shown to be about 11 mW. The data do not extend to high enough powers to clearly indicate whether the first order H-G modes also exhibit saturation, and whether a third set of modes begins to oscillate at still higher drive levels.

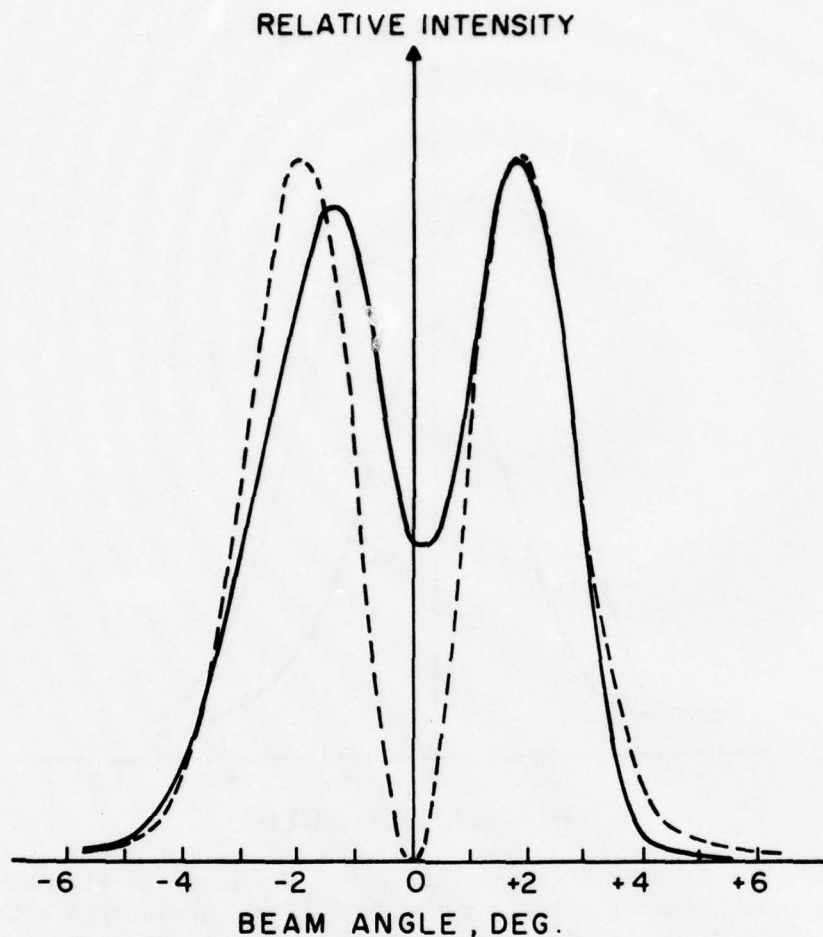


Figure 10. The observed far-field mode pattern of the second lateral mode, after that of the fundamental mode has been subtracted out as explained in the text. The dashed line shows the pattern expected for the first higher-order Hermite-Gaussian mode.

Although, below the kink, the lateral far-field beam pattern and "simple" saturation behavior are consistent with a single oscillating mode, this region is characterized by oscillation of about 60 longitudinal modes. This is true, not only at high power levels near the kink, but down to as close to threshold as we could experimentally measure. Thus, a very large number of longitudinal modes, all with the same lateral (and transverse) mode pattern, begin to oscillate essentially simultaneously at threshold. Indeed, even at power levels as high as our data went above the kink, the same number of fundamental Gaussian modes were observed.

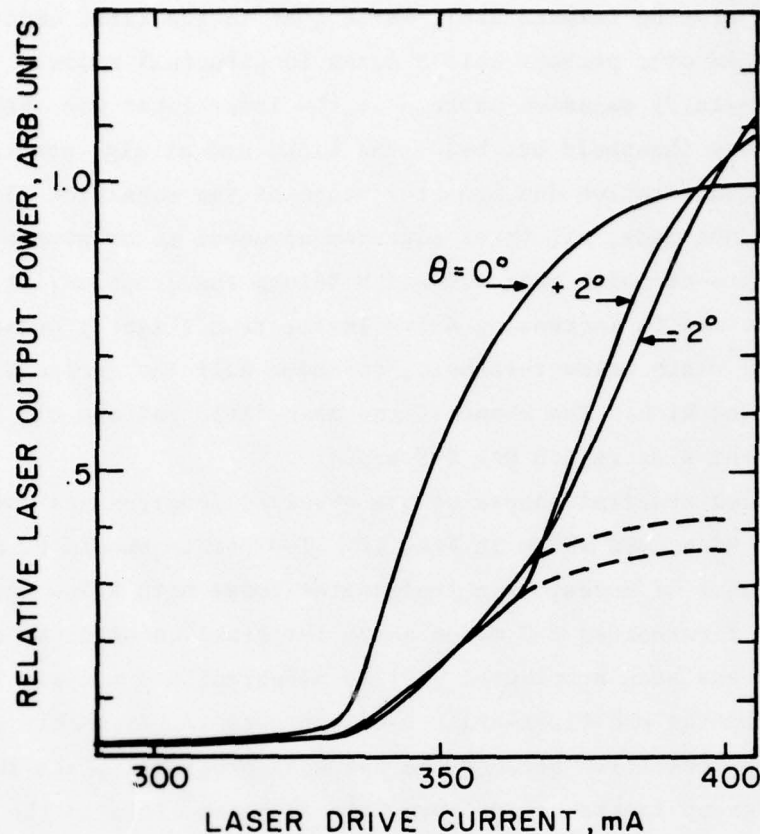


Figure 11. Relative power output curves for the laser of Fig. 8 taken at three angles (in the far-field) with respect to the laser beam axis. The dashed lines are an extrapolation of the off-axis single-mode parts of the curves into the two-mode regions. The power saturation in the fundamental lateral mode is evident.

At the power level of the kink, and higher, a second set of longitudinal modes appeared in the spectrum. These modes, associated with the first-order H-G far-field pattern, have essentially the same longitudinal mode separation and total spectral extent (from about 800.5 nm to roughly 811.5 nm) as the fundamental modes, but the *envelope* of mode intensities was centered at shorter wavelengths, by about 0.8 nm. As seen from Figs. 8 and 11, the total power of these "first-order H-G modes" approximately equals that in the (saturated) fundamental modes at a total output of 24 mW. At this power level, however, most of the energy in the fundamental modes is concentrated

in a single longitudinal mode (or, in two adjacent modes, depending on the exact laser operating temperature), while that in the first order H-G modes was still spread over perhaps half a dozen longitudinal modes.

The (near-field) emission pattern at the laser facet was observed below threshold, above threshold but below the kink, and at high powers above the kink. While quantitative densitometer scans of the magnified TV monitor pictures were not made, all three patterns appeared to be simple Gaussian, the only difference being that the width (along the junction) of the emitting region *decreased* with increasing drive level, from slightly greater than the contact stripe width below threshold, to under half the stripe width at high powers above the kink. The shape of the near-field pattern did not appear to change as the kink region was traversed.

The detailed spectral shapes of the observed longitudinal modes, above and below the kink, are shown in Fig. 12. Two points should be noted. One is that both sets of modes, (the fundamental modes both below and above the kink, and the first-order H-G modes above the kink), show clear structure of the type that has been attributed [10] to different H-G modes. The structure in both fundamental and first-order H-G mode sets is remarkably similar. The wavelength separation between the two most prominent peaks in each longitudinal mode group is about 0.02 nm. This is quite close to the value of 0.017 nm predicted [10] for the separation between the fundamental and first-order H-G modes in our laser. However, the separation between the modes of the fundamental and first-order H-G groups, i.e., between the corresponding members of the two longitudinal mode sets thus identified above, is seen to be approximately 0.08 μm . This spacing cannot be explained on an H-G mode picture.

Another observation should be noted. In increasing the laser output power from below threshold to 24 mW, each observed mode did not shift significantly in wavelength; modes near 807 nm shifted about 0.01 nm toward longer wavelengths, while modes near 805 nm shifted somewhat more, but still only about 0.06 nm in the same direction.

This laser is oscillating in groups of longitudinal modes. The members of each group have essentially the same threshold (despite spreading over a spectral range of over 10 nm) and the same far-field radiation pattern. The onset of oscillation of each such group is accompanied by a sharp rise (and

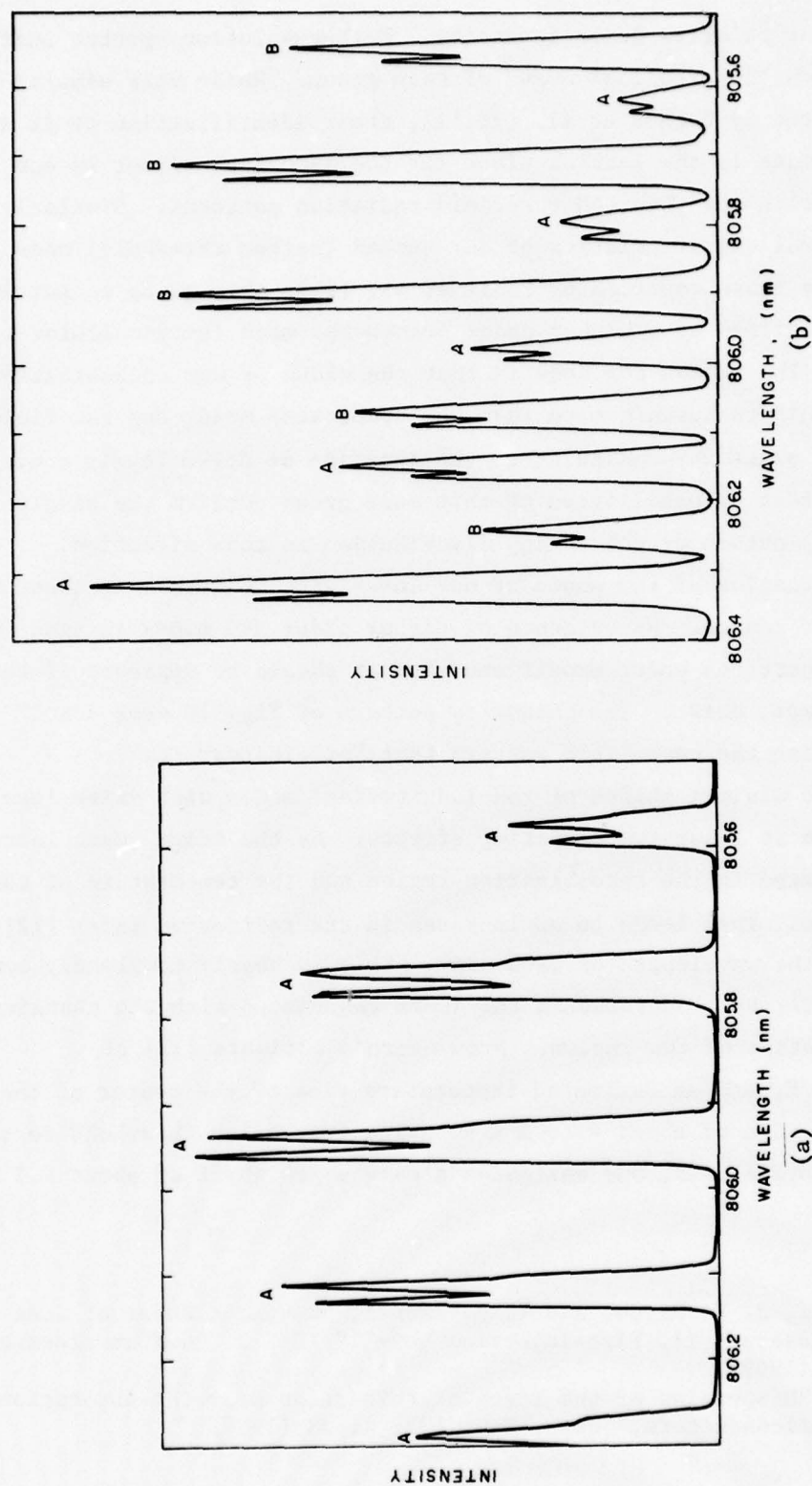


Figure 12. Optical spectra of the laser of Fig. 8 at two power levels. (a) Output power 6 mW, (below kink). Only longitudinal modes associated with the fundamental lateral mode (A) are seen. (b) Output 16 mW, (above kink). Longitudinal modes associated with both the fundamental lateral mode (A) and first higher order lateral mode (B) are seen.

then drop) of the relative noise intensity. High-resolution spectra indicate structure on each "longitudinal mode" of each group. While very similar to structure reported by Zachos et al. [10,11], their identification of it with different H-G modes in the lateral plane (of the junction) cannot in our case be reconciled with our observed far-field radiation patterns. Similarly, while the spectral characteristics of our second (higher threshold) mode group closely resemble those reported by Paoli et al. [11], this group cannot in our case be identified as a higher order *transverse* mode (perpendicular to the junction). The reason for this is that the width of our recombination region is too thin to sustain more than one transverse mode, and far-field patterns in the plane perpendicular to the junction at drive levels above and below the onset of oscillation of this mode group confirm the single (quasi-Gaussian) nature of the energy distribution in this direction.

The identification of the modes of our laser with H-G modes is questionable for another reason. No evidence of higher order H-G modes is seen in the near-field patterns under conditions when it should be apparent if such modes did, in fact, exist. The *intensity* pattern of Fig. 10 does not uniquely determine the near-field pattern that "originates" it.

The observed minimal shifts of the longitudinal modes with drive level must result from at least two competing effects. As the drive level increases, the heat dissipated in the recombination region and the temperature of this region also rise. This leads to an increase in the refractive index [12], and an increase in the wavelength of each mode. This is nearly completely compensated, however, by a decrease in the index associated with the changing gain characteristics of the region. From Stern's estimate [12] of $\frac{dn}{dT} \approx 3.1 \times 10^{-4}/K$, and an estimated temperature rise of the center of the recombination region of about 4 to 5 K in going from below threshold to the highest drive levels used, one estimates a wavelength shift of about 0.3 nm.

11. T. L. Paoli, J. E. Ripper and T. H. Zachos, "Resonant Modes of GaAs Junction Lasers - II. High-Injection Level," IEEE J. Quantum Electron. QE-5, 271 (1969).
12. F. Stern, "Dispersion of the Index of Refraction Near the Absorption Edge of Semiconductors," Phys. Rev. 133, A1653 (1964).

Most of this must be compensated by the decrease in index associated with the gain. On the other hand, the wavelength of peak emission should increase by about 0.23 nm/K [13] due to heating, apart from any band-filling effects, which would tend to reduce this value. Figure 13 shows this behavior; the wavelength of maximum emission for the fundamental modes is plotted as a function of laser drive current. A linear shift is seen, followed, at higher drive currents, by a sublinear rise that can be attributed to band-filling. The slope of Fig. 13 at low drive is somewhat higher than expected, but is within the uncertainties associated with the estimate of this parameter.

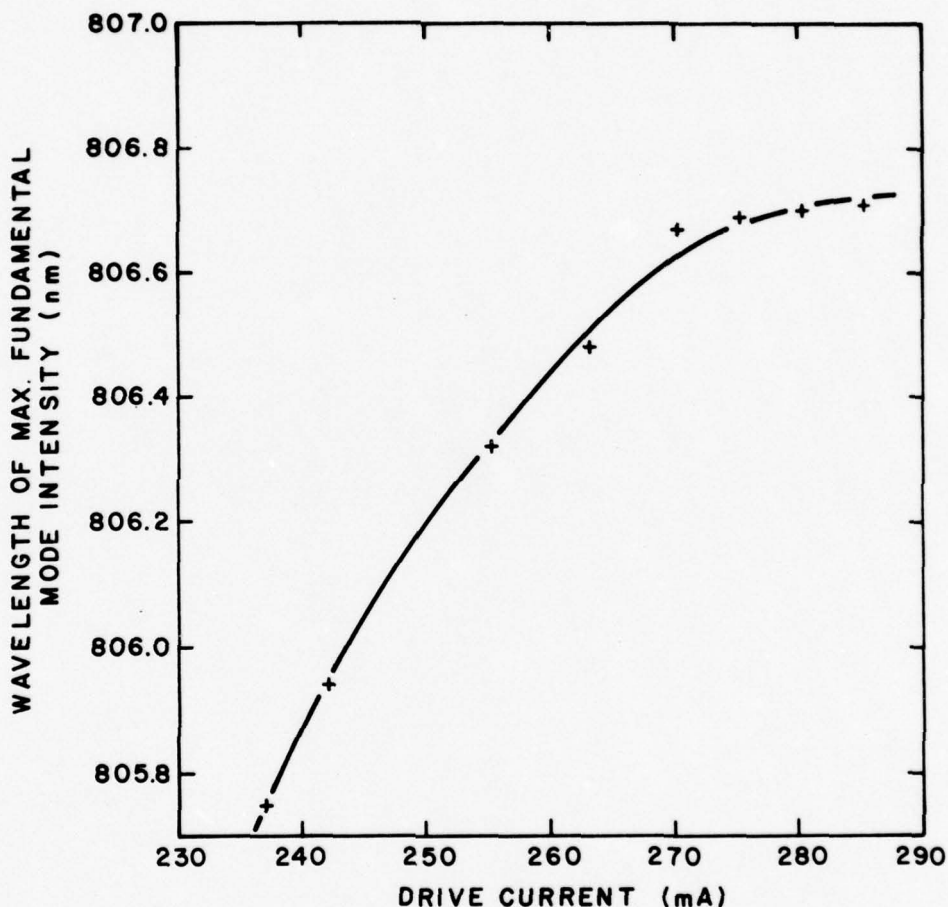


Figure 13. Wavelength of the longitudinal mode of maximum intensity in the fundamental lateral mode as a function of laser drive current.

13. M. B. Panish and H. C. Casey, "Temperature Dependence of the Energy Gap in GaAs and GaP," J. Appl. Phys. 40, 163 (1969).

With a stripe-contact geometry, the temperature is greatest at the lateral center of the region, falling off somewhat to each side. This can play a significant role in determining the lateral refractive index profile, as well as the gain-dependent effects postulated by Hakki [14]. It would explain why the width of the near-field pattern contracts as the drive level is increased.

-
14. B. W. Hakki, "Striped GaAs Lasers: Mode Size and Efficiency," J. Appl. Phys. 46, 2723 (1975).

SECTION V

RADIATION COUPLING

The single-mode fiber supplied by NELC (Naval Electronics Laboratories Center) for the work on this contract was manufactured by Corning Glass Co. It was a high-silica, step-index fiber with a core diameter of approximately 7.5 μm .^{*} Measurements with a laser at 806 nm showed that the transmitted beam gave a roughly Gaussian far-field pattern of 5.3° FWHM, as shown in Fig. 14. This corresponds to a numerical aperture of $\text{NA} = 0.046$; however, for a single-mode fiber, the numerical aperture concept loses much of its validity. Moreover, the fundamental HE_{11} fiber mode does not have a Gaussian far-field pattern. Since exact calculations are extremely tedious, and good insight into coupling and other problems can be achieved by making the simplifying assumption that both laser and fiber modes are strictly Gaussian, we will make this approximation in all that follows.

The half-maximum intensity mode width in the fiber for this far-field pattern is 7.9 μm , or about the core diameter, indicating significant penetration of the propagating fields into the cladding. The lasers used had far-field beam patterns of about 40° FWHM in a plane perpendicular to the diode heterojunctions, and from 5 to 10° in the junction plane. Assuming fundamental Gaussian modes, the beam waist in the laser has a height of about 1.0- μm FWHM, and a width, (for a 7° beam), of 5.9- μm FWHM.

As is discussed below, the fiber end was typically spaced 20 to 30 μm from the laser facet. The question arises, does this put the fiber end in the near or far field of the laser? A Gaussian beam spreads [15] as

$$I = I_0 \exp \left[-\left(\frac{r}{w} \right)^2 \right] \quad (6)$$

^{*}Measurement made by the manufacturer.

15. H. Kogelnik and T. Li, "Laser Beams and Resonators," Proc. IEEE 54, 1312 (1966)

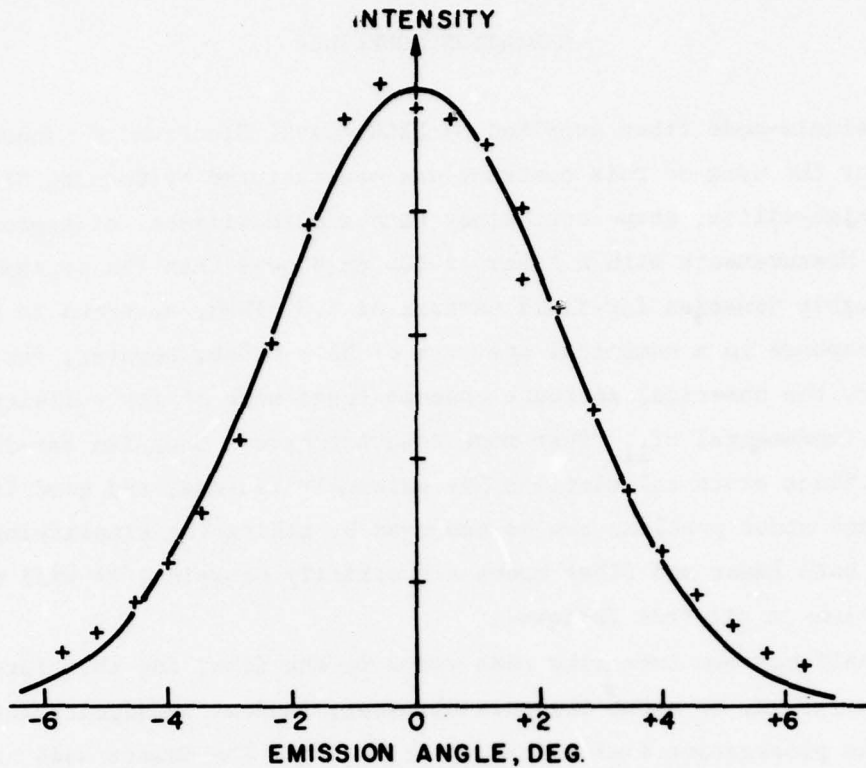


Figure 14. Measured beam profile of radiation transmitted through a section of mode-stripped single-mode fiber, taken at 806 nm using a cw injection laser. The data points represent the measured profile scanned across the center of the far-field radiation pattern; the solid curve shows a Gaussian profile.

where

$$w = w_0 \sqrt{1 + \left(\frac{\lambda z}{\pi w_0^2} \right)^2}, \quad (7)$$

Here, w is the beam-width parameter (see Eq. (6)), w_0 is the beam-width parameter at the beam waist, and z is the distance from the beam waist to where the beam-width parameter is w . In the far field, $\frac{\lambda z}{\pi w_0^2} \gg 1$ and

$$w \approx \frac{\lambda z}{\pi w_0} \quad \text{or} \quad (8)$$

$$\theta_{1/2} = \sqrt{\ln 2} \cdot \frac{w}{z} = \sqrt{\frac{\ln 2}{\pi}} \cdot \frac{\lambda}{w_0} \quad (9)$$

The corresponding width (FWHM) of the waist is

$$d = 2\sqrt{\ln 2} w_0 = \frac{2 \ln 2}{\pi} \frac{\lambda}{\theta_{1/2}} = 0.441 \cdot \frac{\lambda}{\theta_{1/2}} \quad (10)$$

The "far-field region" is where the second term in the radical of Eq. (7) dominates; i.e., where

$$z > \frac{\pi w_0^2}{\lambda} = \frac{\ln 2}{\pi} \cdot \frac{\lambda}{\theta_{1/2}^2} = 0.221 \frac{\lambda}{\theta_{1/2}^2} \quad (11)$$

For the laser beam angle $\theta_{1/2} = 20^\circ$, this becomes

$$z_{ff} (\theta_{1/2} = 20^\circ) > 1.5 \mu\text{m} \quad (12)$$

For the narrower laser beam angle in the plane of the junction,

$$z_{ff} (\theta_{1/2} = 3.5^\circ) > 48.6 \mu\text{m}. \quad (13)$$

Thus, we see that, as far as the narrow 7° beam angle is concerned, the fiber end is not in the far field, and that the near-field laser pattern is quite a good match to the fiber mode. Coupling of the fundamental laser mode to the fiber mode should therefore be quite good in this plane, limited primarily by how closely the fiber end can be mounted to the laser facet. In the perpendicular (40° beam angle) direction, we are clearly in the far field, and a (cylindrical) lens can, in principle, significantly increase the coupling by reducing the angular beam spread to more nearly match the acceptance cone of the fiber. Since the effective laser size in this direction ($1.0 \mu\text{m}$) is roughly 5 times smaller than the effective core height, a lens with a 5X magnification could be used. However, if the fiber end (or lens surface) must be kept 20 to $30 \mu\text{m}$ from the laser facet for safety reasons, the lens surface must then be 100 to $150 \mu\text{m}$ from the end of the fiber. This would greatly reduce the coupling in the other plane, and is not desirable.

It is possible that a tapered transition [16] could be used to increase the coupling between laser and fiber. Since what was considered adequate coupling, discussed below, was achieved by merely bringing a cleaved fiber end into close proximity with the laser facet, the tapered transition was not explored in this contract.

With the emitting laser area of the fundamental mode about $1 \times 6 \mu\text{m}$, its positioning relative to the $7.5\text{-}\mu\text{m}$ fiber core is critical. Figure 15 shows how the coupling varied for two of our lasers for displacements of the fiber end parallel, and perpendicular, to the junction plane; Fig. 15(a) shows the results for a laser with a $5\text{-}\mu\text{m}$ -stripe electrical contact, and Fig. 15(b), for a $13\text{-}\mu\text{m}$ -stripe. The -3 dB displacements are seen to be essentially the same, $\sim 6 \mu\text{m}$, for displacements perpendicular to the junction planes. Parallel to the junction plane, there is a faster coupling fall-off with displacement for the narrower stripe laser, but the effect is small. This is not surprising, since the above estimate of the (Gaussian) mode width, $\sim 6 \mu\text{m}$, applied to both lasers: the wider laser presumably can sustain more modes, but these do not couple efficiently to the fiber mode. Although the -3 dB points correspond to displacements of $\pm 3 \mu\text{m}$, coupling decreases even at smaller deviations from optimum alignment. It is clear that maintenance of relative position to tolerances of the order of $\pm 1 \mu\text{m}$ is required.

The coupling efficiency as a function of laser power level is shown in Fig. 16 for the $5\text{-}\mu\text{m}$ -stripe and $13\text{-}\mu\text{m}$ -stripe lasers. There is no significant difference between the two lasers within the accuracy of the measurements. The $5\text{-}\mu\text{m}$ -stripe laser shows some variation of coupling, and hence, mode pattern, with drive current, whereas the $13\text{-}\mu\text{m}$ -stripe laser appears stable. It is not believed that this observed (small) difference can be reliably attributed to the difference in contact width, but merely represents the range of variation to be expected in a random selection of diodes.

In aligning short lengths of the single-mode fiber, it was found that the thin protective plastic coating applied to the fiber at manufacture had a lower index than the silica fiber cladding, thus forming a "secondary" optical fiber with the entire silica fiber itself acting as core. This

16. D. G. Dalgoutte, G. L. Mitchell, R. L. K. Matsumoto and W. D. Scott, "Transition Waveguides for Coupling Fibers to Semiconductor Lasers," Appl. Phys. Lett. 27, 125 (1975).

"secondary" optical guide could sustain a very large number ($> 10^3$) of modes, and the light coupled into them from the laser completely obscured that coupled into the desired single-core mode, thereby preventing alignment. Mode stripping was clearly needed. The conventional method of removing the plastic and immersing the fiber in a liquid of greater index than silica was rejected as it would leave the fiber without a protective plastic coating after the high-index liquid was removed. Instead, a mode-stripping technique was developed which removed the plastic layer and replaced it with a sprayed acrylic film that formed a somewhat irregular, rather "beaded" film. This effectively coupled out all cladding modes in a few inches, and left the fiber protected, and yet roughly as flexible as before.

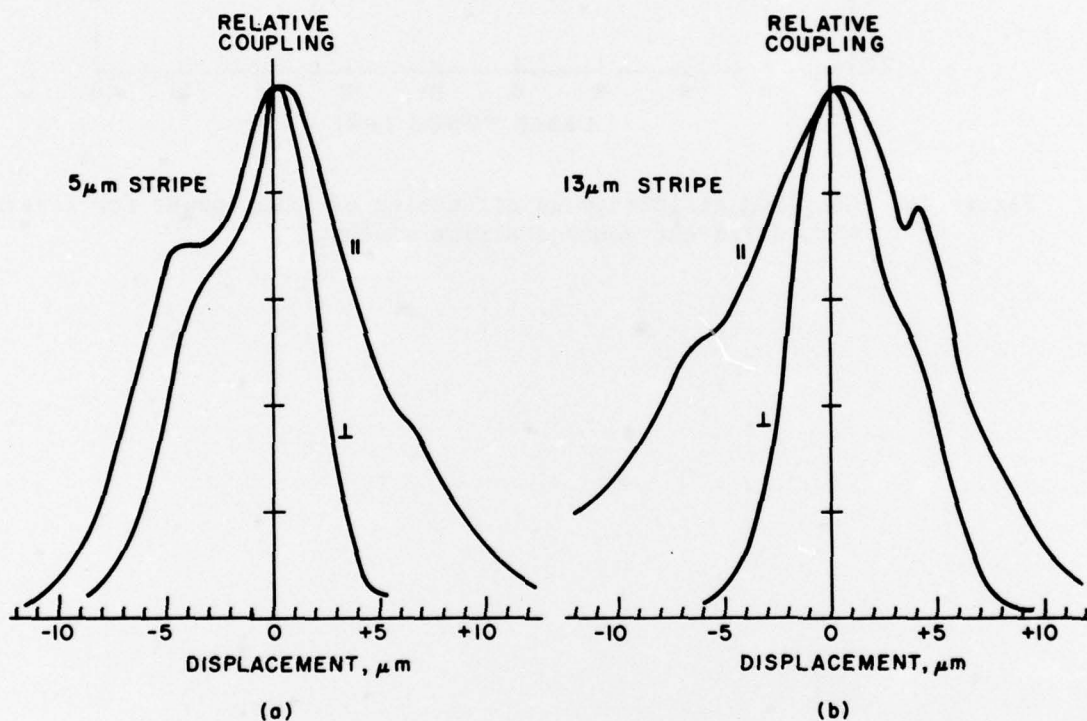


Figure 15. Change of coupling from laser into single-mode fiber as the fiber end is translated perpendicular to the beam axis. Displacement in, ($||$), and perpendicular to, (\perp), the junction plane are shown.

- (a) Coupling variations for a laser with a 5- μm -wide stripe electrical contact;
- (b) Coupling variations for a laser with a 13 μm -wide stripe contact.

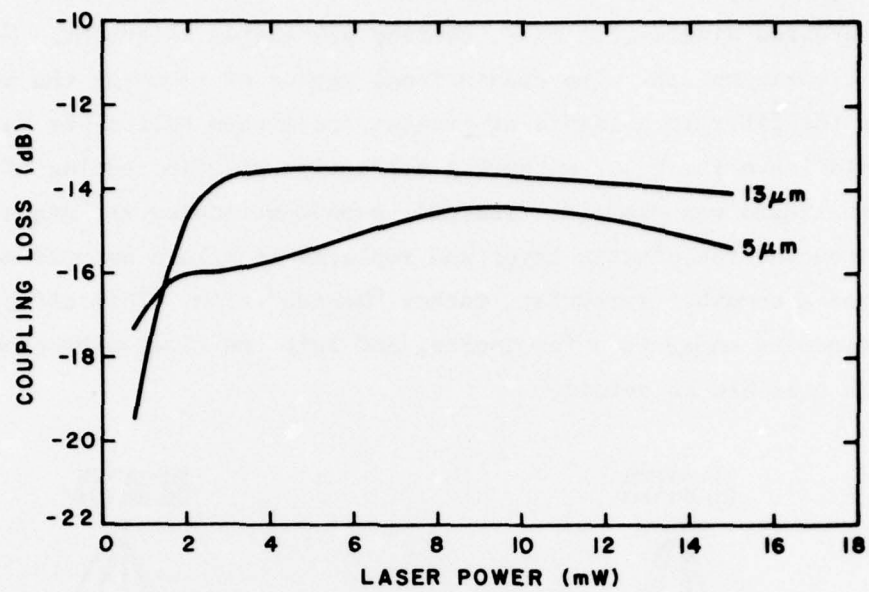


Figure 16. Coupling efficiency as a function of laser power for lasers with different contact stripe widths.

SECTION VI

MECHANICAL CONSIDERATIONS

The package to hold the laser and fiber end in alignment has to meet severe requirements:

1. It must not interfere with the laser cooling (heat sinking).
2. It must hold the relative positions of laser and fiber end to $\pm 1 \mu\text{m}$ for a lengthy period of time.
3. Even though the laser temperature is stabilized, the coupling should not be sensitive to small (\pm a few $^{\circ}\text{C}$) temperature changes.
4. It must be mechanically rugged.
5. It should be as small as possible.

We believe that the package we have developed, shown in Fig. 17, goes far toward meeting these requirements. The fiber is first mounted rigidly to a fiber mounting block, which is then attached to the laser heat sink. This permits the delicate fiber to be easily and rigidly attached to its mount without critical alignment tolerances, which are hard to maintain when adjusting the position of such a mechanically fragile element. After this bond is made, the rugged fiber mounting block can then be maneuvered to align the fiber accurately and be clamped in position while the final bond is made.

As mentioned above, the lateral tolerances in the fiber position are quite severe. Along the laser axis, the requirements are, in a sense, reduced: a motion of a few microns (at a spacing of $20 \mu\text{m}$ between laser facet and fiber end) does not change the coupling by more than a few percent. However, coupling increases monotonically as the fiber approaches the laser, and it therefore is desirable to mount the two as close to each other as is feasible. In practice, we used separations in the 20 to $30\text{-}\mu\text{m}$ range. If the fiber end is allowed to press on the laser facet during alignment, the facet may be damaged, leading either to immediate destruction of the laser, or to a greatly shortened laser lifetime. The alignment was performed under a low-power microscope and experience indicated that it was not safe to make the laser-fiber spacing less than 20 to $30 \mu\text{m}$, even though coupling would be significantly improved at $10 \mu\text{m}$.

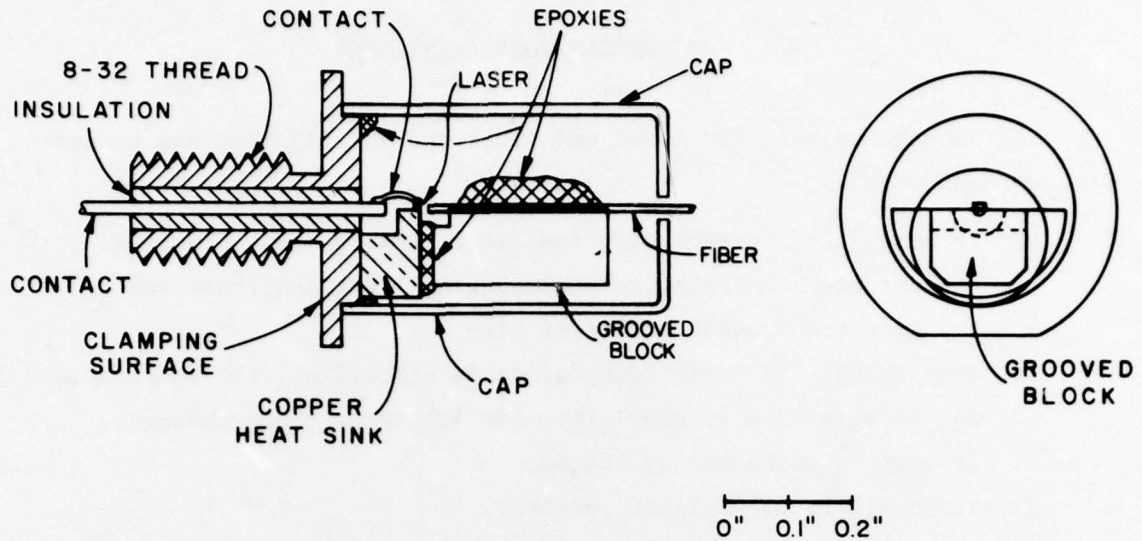


Figure 17. Cross section of the laser-fiber mounting package.

The requirements on the material used to bond the fiber to its mounting block are not too stringent. It must be dimensionally stable after the bond is made, it must be able to bond to the fiber without damaging it, and it must not be disturbed by whatever means are used for the final fiber mount-to-laser heat-sink bond. We have successfully used two bonding materials, a room-temperature-setting epoxy,* and indium metal solder. When the solder was used, the fiber was metallized by a chrome-platinum-gold evaporation with a total thickness of 190 nm before soldering.

The extent to which the fiber end protrudes beyond the end of its mounting block determines how thick the final bonding material must be. One wants to keep this material as thin as possible, to minimize any dimensional changes with time (or temperature) in this bond, but it must be thick enough to permit proper bond curing, etc., and an adequate range of adjustment. A value of 100 to 250 μm was chosen for this spacing, so that the fiber should protrude about 75 to 225 μm past the end of its mounting block. It was easy to maintain this (loose) tolerance in mounting the fiber to the block.

*Metalset[®] A4, manufactured by Smooth-On, Inc., Box 427, Stirling, N.J. 07980.

The geometry of the heat sink and mounting block should be such that thermal and other possible distorting effects are minimized. Ideally, this would suggest a tubular, coaxial mount. However, the exigencies of mounting the laser on its heat sink, and the necessity of optically monitoring the relative laser-fiber spacing during alignment led to the design of Fig. 17. Here, the bond material forms a 100 to 250- μm -thick region that is roughly 0.3 x 0.15 cm in area. With a thermal expansion rate of $10^{-4}/\text{K}$ (for the epoxy bond; the solder bond to be discussed below has a rate only $10^{-5}/\text{K}$, the bond lengthens 1 μm or less for a temperature change of 40°C. The lateral, misaligning shifts should be much less than this, and, hence, should be negligible.

The bond material used in joining the fiber mounting block to the laser heat-sink is critical. Dimensional changes as the bond hardens or ages can destroy the required alignment. Two general types of bond materials were studied, epoxies and low-melting solders. Epoxies have the advantages that they can be applied and can harden (cure) at room temperature, adhere to metals, and form a strong bond. The disadvantages are that they generally take a rather long (>10 h) time to cure, during which the alignment of fiber and laser may be disturbed (by e.g., thermal drifts in the apparatus), and that, in general, their long term (over months) dimensional stabilities are not known. Solders, on the other hand, have the advantage of solidifying rapidly, and they can easily be remelted if something should shift during alignment and bonding, (an impossibility with epoxies), and can be made with excellent long-term dimensional stability [17].

Epoxies were investigated first. Since the laser-fiber bonds are sealed in a protective aluminum can after assembly, no epoxy could be used that gave off condensable, or possibly corrosive, reaction products, such as acetic acid. Thus, several otherwise desirable epoxies had to be rejected. Holographic techniques were used in an attempt to study dimensional change during curing. While these indicated that some epoxies undergo nonuniform dimensional changes on curing, it was not felt that the measurement technique was of adequate sensitivity to guarantee that an epoxy that seemed stable was, in fact, sufficiently so. Actual laser-fiber coupling experiments seemed to provide the most sensitive test available for stability. Our conclusions are that Metalset[®] A4, as noted above, was the best epoxy of those we tested.

17. W. H. Kohl, *Handbook of Materials and Techniques for Vacuum Devices*, (Reinhold Publ. Corp., New York, 1967), Chapter 13.

For a time during the contract period, we had difficulties that we attributed to long-term dimensional changes in the epoxy bonds. For this reason, we also investigated low-temperature solders as bond material. Since indium is used to bond the laser chip to its copper heat sink, the solder obviously had to have a melting temperature significantly below the melting temperature of indium, 155°C. Also, its melting point has to be sufficiently above the highest expected operating temperature so that there was no danger of softening. This gave an allowable range of $50^{\circ} \lesssim T_{\text{melt}} \lesssim 120^{\circ}\text{C}$. Solder compositions having melting points in this range have a tendency to change dimensions while aging after solidification [17]. However, Cerrolow 136^{*} has a melting point of 57°C, and is very dimensionally stable as it ages. Therefore, all solder experiments were made with this material. An assembly jig was built that permitted independent control of laser heat sink and fiber mounting block temperatures and relative positions. Both surfaces to be joined were first "tinned" with the solder, leaving an adequate amount of solder on the surface to form the final bond. Then they were heated above the solder melting point, aligned, and the solder was allowed to solidify, a process that took only a few seconds.

While the soldering technique was relatively easy to apply and gave strong bonds, the final results were unsatisfactory, and we had to revert to the epoxy technique. It is not completely certain what the cause of the difficulty was, but, on cooling to room temperature and subsequent cw laser operation, the laser-fiber coupling was generally found to be quite poor. Two possible causes suggest themselves. One is that the alignment shifts as the solder cools from its solidification temperature to room temperature. This was suggested by some observations made as the system cooled. A shift in the fiber position was observed, but it was uncertain whether or not there was a corresponding shift in the laser position, i.e., whether or not the entire assembly shifted as a unit. The other possibility concerns laser mode changes. Because the laser cannot be operated continuously at the elevated temperatures required for soldering, the alignment was performed under pulsed conditions. Far-field scans of the laser beam pattern, which are a good indication of the

* Manufactured by Cerro Metal Products, Bellefonte, Penna. 16823.

oscillating laser modes, showed no changes in pattern with temperature, as long as the laser output power was kept constant (see Fig. 18). However, as expected, at different output powers, the beam patterns differed significantly. Thus, with these lasers, the coupling can only be optimized at one operating level, because mode-changes with drive current can shift the radiation pattern and the coupling. What led to our abandonment of solder-bonding was the observation that for the lasers tested, at least, room-temperature cw far-field patterns could not be duplicated under *any* pulsed power conditions, as shown in Fig. 19. Thus, one would expect the cw mode structure, and hence, the coupling, to differ between the pulsed, high-temperature alignment condition and the desired cw, room-temperature operating condition. Regardless of alignment shifts on cooling, this alone could explain our variable results.

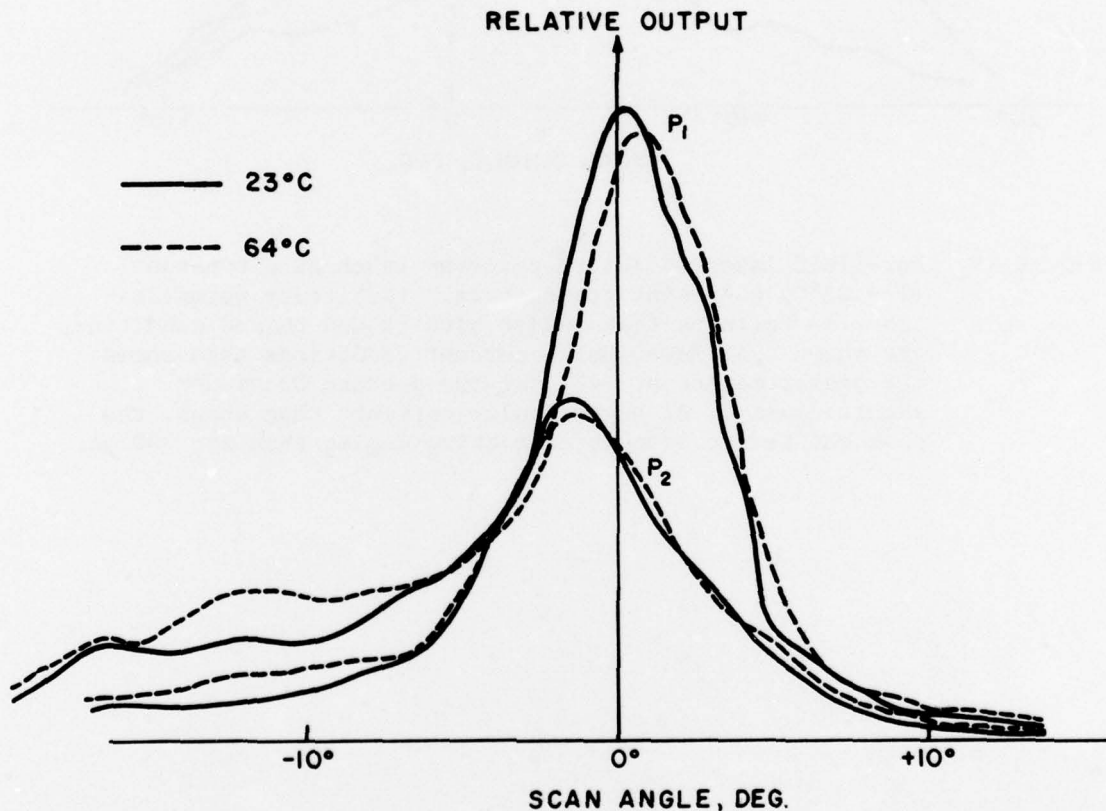


Figure 18. Far-field laser radiation patterns at two different temperatures and peak output powers, taken under pulsed conditions. Pulse length = 0.5 μ s.

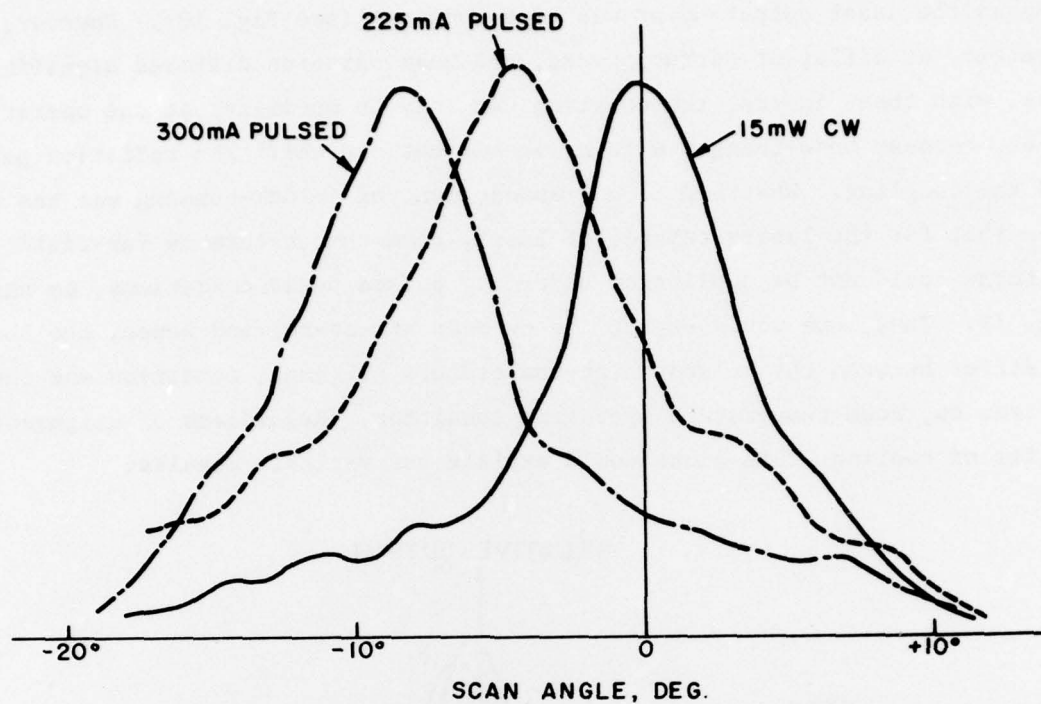


Figure 19. Far-field laser radiation patterns taken at a constant ($T = 23^{\circ}\text{C}$) heat-sink temperature. (Arbitrary normalizations.) Patterns taken under both cw and pulsed conditions are shown. At lower pulse current conditions than shown, the peak remained at -4° , but the pattern broadened significantly. At higher pulse currents than shown, the peak shifted to even more negative angles than for 300 mA.

SECTION VII

FIBER-LASER ASSEMBLIES: RESULTS

The lasers used for the final samples had a contact width of $\sim 13 \mu\text{m}$. Since, as mentioned above, approximately $1 \text{ mW}/\mu\text{m}$ is a safe-operating, optical flux density level at the emitting facet, these lasers can be safely operated at a $\sim 13\text{-mW}$ power level. However, occasionally, lasers operated at this power level, while showing no threshold increase or other obvious evidence of degradation, did exhibit a change in mode pattern as evidenced by an altered far-field pattern. To ensure against such modal shifts which can change the coupling efficiency into the single-mode fiber, we have found it desirable to limit operation to about a 10-mW level. At this flux density, we have not observed any modal shifts, with properly "aged" diodes.

The coupling efficiency from laser into single-mode fiber was seen (Fig. 16) to be about -15 dB , or a factor of 32. This is roughly what is expected from the $\sim 5\text{-dB}$ loss anticipated with the width of the emitting region ($\sim 20 \mu\text{m}$) being approximately three times the core diameter, and also the $\sim 9\text{-dB}$ loss expected from the 40° transverse-plane beam angle and the 5.3° acceptance angle of the fiber, since the fiber end is in the far-field region in the transverse direction. At a 10-mW laser output level, this then corresponds to about $300 \mu\text{W}$ coupled into the fiber. This is what was observed. Power curves through the mode-stripped, single-mode fiber are shown in Figs. 20 and 21 for two of our better, packaged units. Diode A (Fig. 20) shows a nearly linear characteristic and about $450\text{-}\mu\text{W}$ coupled power at a drive current corresponding to 10 mW from the entire laser facet. Diode H (Fig. 21) shows, in its curved characteristic, the effects of more than one laser mode oscillating and being coupled into the fiber, showing a coupled power of $600 \mu\text{W}$ at a 10-mW drive. Other units did not show as great a transmitted power level, but units with $>150 \mu\text{W}$ coupled powers could regularly be made. The lower power levels were associated with optical misalignments, due either to position shifts during the curing of the epoxy bonds, or, less likely, mode shifts in the lasers.

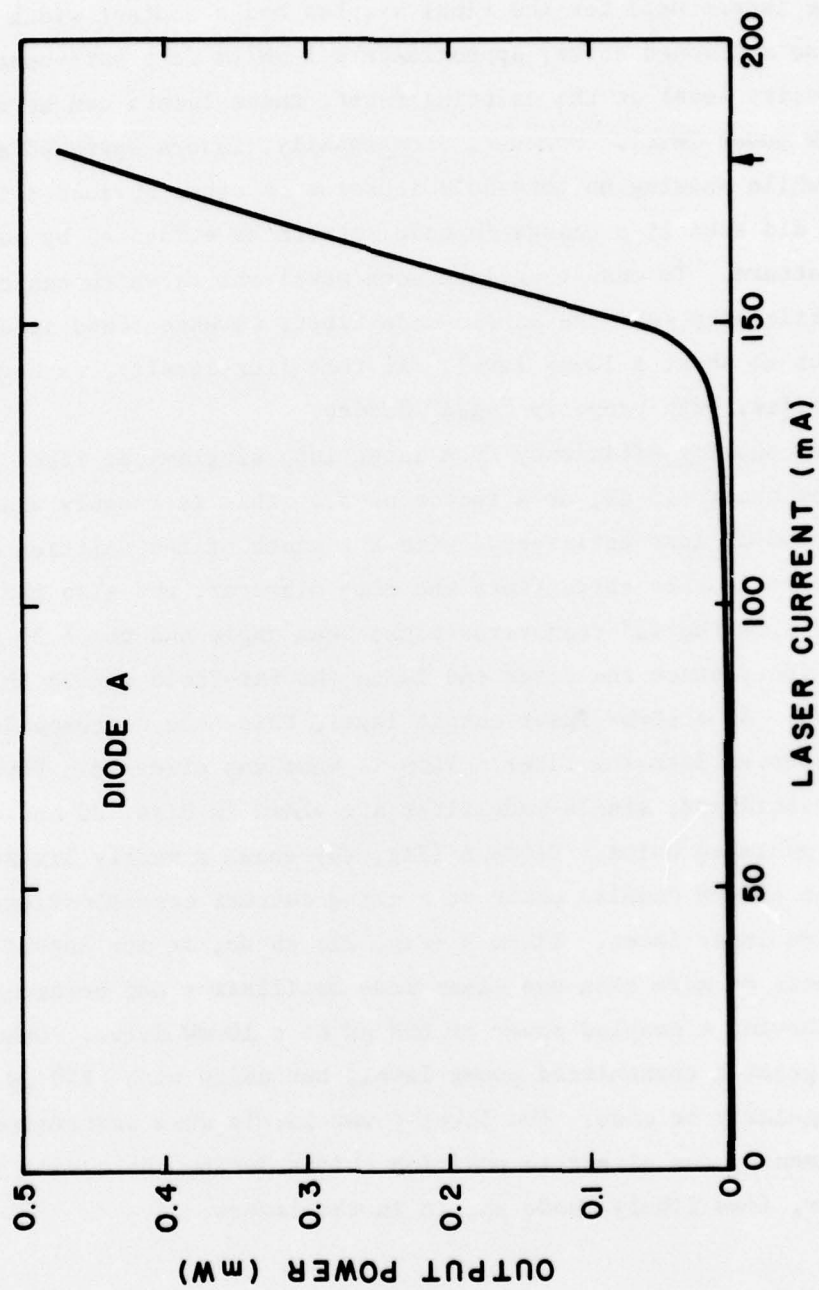


Figure 20. Output power through a coupled single-mode fiber for one laser-fiber unit.
A current of 180 mA corresponds to a total laser output power of 10 mW.

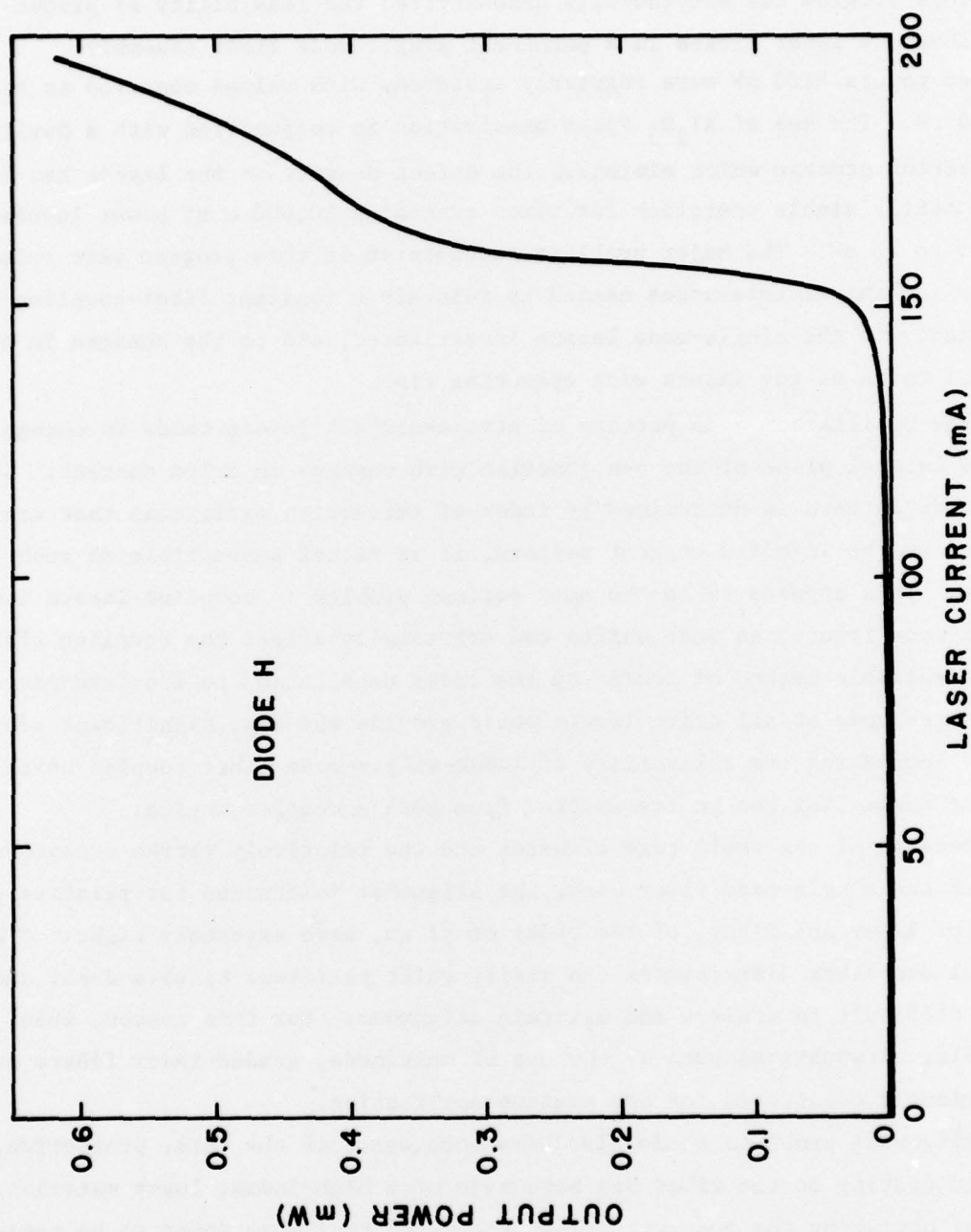


Figure 21. Output power through a coupled single-mode fiber for a second laser-fiber unit. A current of 195 mA corresponds to a total laser output of 10 mW.

SECTION VIII

CONCLUSIONS

This program has successfully demonstrated the feasibility of producing AlGaAs cw laser diodes in a permanent single-mode fiber assembly. Coupled powers $>150 \mu\text{W}$ were regularly achieved, with values observed as high as $600 \mu\text{W}$. The use of Al_2O_3 facet passivation in conjunction with a device fabrication process which minimizes the defect density in the lasers has led to consistently stable operation for times exceeding 10,000 h at power levels from 5 to 15 mW. The major problems encountered in this program were related to the mechanical tolerances needed to maintain a constant fiber-coupling efficiency in the single-mode lasers investigated, and to the changes in the lateral modes of the lasers with operating time.

The oscillation mode pattern of stripe-contact lasers tends to change in the lateral plane of the p-n junction with changes in drive current. Since this mode pattern is determined by index of refraction variations that are induced by the injected current pattern, it is rather susceptible to such shifts. This appears to be the most serious problem in coupling lasers into single-mode fibers, as mode shifts can drastically affect the coupling efficiency. A reliable method of confining the laser oscillation to its fundamental transverse mode at all drive levels would provide the most significant advance toward increasing the reliability of laser-single-mode fiber coupled units, and the power that can be transmitted from such a coupled device.

Because of the small core diameter and the relatively narrow acceptance cone of the single-mode fiber used, the alignment tolerances for relative positions of laser and fiber, of the order of $\pm 1 \mu\text{m}$, were extremely tight. Since thermal and other disturbances can easily shift positions by this small amount, it is difficult to achieve and maintain alignment. For this reason, when possible, alternatives such as the use of multimode, graded-index fibers should be seriously considered for any systems application.

Alignment problems would also have been eased if the thin, protective, plastic coating on the fiber had been made of a high-index, lossy material, thereby obviating the mode-stripping procedures that were found to be necessary.

The long-term alignment stability of the laser-fiber combination depends on the long-term dimensional stability of the bonding epoxy. This is not known at present. The stability of suitable, low-melting solders is believed to be adequate for this bonding. However, to avoid the difficulties we experienced in the work under this contract, in trying to use solders as binding materials, innovative approaches would be required. One possibility would be to use a thin, metallized, ceramic spacer between the laser heat sink and the fiber mounting block. This could supply the required thermal isolation between the molten solder bond and the laser, permitting cw operation of the laser during alignment.

REFERENCES

1. I. Ladany and H. Kressel, "Influence of Device Fabrication Parameters on Gradual Degradation of (AlGa)As CW Laser Diodes," Appl. Phys. Lett. 25, 708 (1974).
2. I. Ladany, "The Influence of Stripe Width on the Threshold Current of DH Lasers," J. Appl. Phys. (to be published).
3. H. Kressel and I. Ladany, "Reliability Aspects and Facet Damage in High-Power Emission from (AlGa)As CW Laser Diodes at Room Temperature," RCA Rev. 36, 230 (1975).
4. I. Ladany, M. Ettenberg, H. F. Lockwood, and H. Kressel, "Al₂O₃ Half-Wave Films for Long-Life CW Lasers," Appl. Phys. Lett. 30, 87 (1977).
5. T. Tsukada, "GaAs-Ga_{1-x}Al_xAs Buried-Heterostructure Injection Lasers," J. Appl. Phys. 45, 4898 (1974).
6. T. L. Paoli, "Noise Characteristics of Stripe-Geometry Double-Heterostructure Junction Lasers Operating Continuously - I. Intensity Noise at Room Temperature," IEEE J. Quantum Electron. QE-11, 276 (1975).
7. D. E. McCumber, "Intensity Fluctuations in the Output of CW Laser Oscillators-I," Phys. Rev. 141, 306 (1966).
8. T. L. Paoli and J. E. Ripper, "Observation of Intrinsic Quantum Fluctuations in Semiconductor Lasers," Phys. Rev. 2A, 2551 (1970).
9. J. A. Armstrong and A. W. Smith, "Intensity Fluctuations in GaAs Laser Emission," Phys. Rev. 140, A155 (1965).
10. T. H. Zachos and J. E. Ripper, "Resonant Modes of GaAs Junction Lasers," IEEE J. Quantum Electron. QE-5, 29 (1969).
11. T. L. Paoli, J. E. Ripper and T. H. Zachos, "Resonant Modes of GaAs Junction Lasers - II. High-Injection Level," IEEE J. Quantum Electron. QE-5, 271 (1969).
12. F. Stern, "Dispersion of the Index of Refraction Near the Absorption Edge of Semiconductors," Phys. Rev. 133, A1653 (1964).
13. M. B. Panish and H. C. Casey, "Temperature Dependence of the Energy Gap in GaAs and GaP," J. Appl. Phys. 40, 163 (1969).
14. B. W. Hakki, "Striped GaAs Lasers: Mode Size and Efficiency," J. Appl. Phys. 46, 2723 (1975).
15. H. Kogelnik and T. Li, "Laser Beams and Resonators," Proc. IEEE 54, 1312 (1966).
16. D. G. Dalgoutte, G. L. Mitchell, R. L. K. Matsumoto and W. D. Scott, "Transition Waveguides for Coupling Fibers to Semiconductor Lasers," Appl. Phys. Lett. 27, 125 (1975).
17. W. H. Kohl, *Handbook of Materials and Techniques for Vacuum Devices*, (Reinhold Publ. Corp., New York, 1967), Chapter 13.